

EXTRAGALACTIC BACKGROUND LIGHT FROM HIERARCHICAL GALAXY FORMATION: GAMMA-RAY ATTENUATION UP TO THE EPOCH OF COSMIC REIONIZATION AND THE FIRST STARS

YOSHIYUKI INOUE¹, SUSUMU INOUE^{2,3}, MASAKAZU A. R. KOBAYASHI⁴, RYU MAKIYA⁵, YUU NIINO⁶, & TOMONORI TOTANI⁵

¹Kavli Institute for Particle Astrophysics and Cosmology, Department of Physics, Stanford University and SLAC National Accelerator Laboratory, 2575 Sand Hill Road, Menlo Park, CA 94025, USA

²Max-Planck-Institut für Kernphysik, Saupfercheckweg 1, 69117 Heidelberg, Germany

³Institute for Cosmic Ray Research, University of Tokyo, Kashiwa, Chiba 277-8582, Japan

⁴Research Center for Space and Cosmic Evolution, Ehime University, Bunkyo-cho, Matsuyama 790-8577, Japan

⁵Department of Astronomy, Kyoto University, Sakyo-ku, Kyoto 606-8502, Japan and

⁶Optical and Infrared Astronomy Division, National Astronomical Observatory of Japan, Mitaka, Tokyo 181-8588, Japan

Draft version November 27, 2024

ABSTRACT

We present a new model of the extragalactic background light (EBL) and corresponding $\gamma\gamma$ opacity for intergalactic gamma-ray absorption from $z = 0$ up to $z = 10$, based on a semi-analytical model of hierarchical galaxy formation that reproduces key observed properties of galaxies at various redshifts. Including the potential contribution from Population III stars and following the cosmic reionization history in a simplified way, the model is also broadly consistent with available data concerning reionization, particularly the Thomson scattering optical depth constraints from *WMAP*. In comparison with previous EBL studies up to $z \sim 3\text{--}5$, our predicted $\gamma\gamma$ opacity is in general agreement for observed gamma-ray energy below $400/(1+z)$ GeV, whereas it is a factor of ~ 2 lower above this energy because of a correspondingly lower cosmic star formation rate, even though the observed UV luminosity is well reproduced by virtue of our improved treatment of dust obscuration and direct estimation of star formation rate. The horizon energy at which the gamma-ray opacity is unity does not evolve strongly beyond $z \sim 4$ and approaches ~ 20 GeV. The contribution of Population III stars is a minor fraction of the EBL at $z = 0$, and is also difficult to distinguish through gamma-ray absorption in high- z objects, even at the highest levels allowed by the *WMAP* constraints. Nevertheless, the attenuation due to Population II stars should be observable in high- z gamma-ray sources by telescopes such as *Fermi* or CTA and provide a valuable probe of the evolving EBL in the rest-frame UV. The detailed results of our model are publicly available in numerical form at the URL <http://www.slac.stanford.edu/%7eyinoue/Download.html>.

Subject headings: cosmology: diffuse radiation – gamma rays : theory – galaxies: evolution

1. INTRODUCTION

The extragalactic background light (EBL), the diffuse, isotropic background radiation from far-infrared (FIR) to ultraviolet (UV) wavelengths, is believed to be predominantly composed of the light from stars and dust integrated over the entire history of the Universe (see Dwek & Krennrich 2012, for reviews). The observed spectrum of the local EBL at $z = 0$ has two peaks of comparable energy density. The first peak in the optical to the near-infrared (NIR) is attributed to direct starlight, while the second peak in the FIR is attributed to emission from dust that absorbs and reprocesses the starlight.

The precise determination of the EBL has been a difficult task. Direct measurements of the EBL in the optical and NIR bands have been hampered by bright foreground emission caused by interplanetary dust, the so-called zodiacal light (see Hauser & Dwek 2001, for reviews). Recently, Matsuoka et al. (2011) reported measurements of the EBL at $0.44 \mu\text{m}$ and $0.65 \mu\text{m}$ from outside the zodiacal region using observational data from *Pioneer 10/11*. On the other hand, integration over galaxy number counts provide a firm lower bound on the EBL, and the observed trend of the counts with magnitude indicates that the EBL at $z = 0$ has been largely resolved into discrete sources in the optical/NIR bands (e.g. Madau & Pozzetti 2000; Totani et al. 2001; Keenan et al. 2010), even when the effect of incomplete detection due to cosmological dimming of surface brightness is taken into account (Totani et al. 2001).

The EBL can also be probed indirectly through observations of high-energy gamma rays from extragalactic objects (e.g. Gould & Schröder 1966; Jelley 1966; Stecker et al. 1992; Mazin & Raue 2007). Gamma-rays propagating through intergalactic space can be attenuated by photon-photon pair production interactions ($\gamma\gamma \rightarrow e^+e^-$) with low-energy photons of the EBL. For gamma-rays of given energy E_γ , the pair production cross section peaks for low-energy photons with energy

$$\epsilon_{\text{peak}} \simeq \frac{2m_e^2 c^4}{E_\gamma} \simeq 0.5 \left(\frac{1 \text{ TeV}}{E_\gamma} \right) \text{ eV}, \quad (1)$$

where m_e is the electron mass and c is the speed of light. In terms of wavelength, $\lambda_{\text{peak}} \simeq 2.5(E_\gamma[\text{TeV}]) \mu\text{m}$. Measuring the resultant attenuation features in the spectra of extragalactic GeV-TeV sources would offer a valuable probe of the EBL that is indirect, yet unique in being redshift-dependent. Although this method can be limited by incomplete knowledge of the intrinsic spectra of the source before attenuation, by assuming a plausible range for such spectra, observations of blazars by current ground-based telescopes have been able to place relatively robust upper limits to the EBL at $z = 0$ and up to $z \sim 0.5$ (e.g. Aharonian et al. 2006a; Albert et al. 2008). This has been complemented by *Fermi* observations of blazars and gamma-ray bursts (GRBs) that placed upper limits on the $\gamma\gamma$ opacity up to $z = 4.35$ (Abdo et al. 2009, 2010a). The energy density of the local EBL has been constrained to be $< 24 \text{ nW m}^{-2} \text{ sr}^{-1}$ at optical wavelengths, and

$< 5 \text{ nW m}^{-2} \text{ sr}^{-1}$ between $8 \mu\text{m}$ and $31 \mu\text{m}$ (Meyer et al. 2012). Combined with the lower limits from galaxy counts, the total EBL intensity at $z = 0$ from $0.1 \mu\text{m}$ to $1000 \mu\text{m}$ is inferred to lie in the range $52\text{--}99 \text{ nW m}^{-2} \text{ sr}^{-1}$ (Horiuchi et al. 2009). Very recently, HESS has succeeded in positively measuring the imprint of the local EBL in the spectra of bright blazars, assuming only that their intrinsic spectra have smooth shapes (Abramowski et al. 2013). *Fermi* has also positively detected the redshift-dependent signature of EBL attenuation up to $z = 1.5$, utilizing the collective spectra of a large number of blazars (Ackermann et al. 2012). However, the EBL at higher redshifts is still highly uncertain.

Currently available theoretical models for the EBL can be broadly categorized into three types. First, in backward evolution models, one starts from the observed properties of galaxies in the local Universe and describes their evolution by extrapolating backwards in time in a parameterized fashion (e.g. Malkan & Stecker 1998; Totani & Takeuchi 2002; Stecker et al. 2006; Franceschini et al. 2008). This extrapolation entails uncertainties in the properties of the EBL that inevitably increase at high redshifts. Nevertheless, based on the observed, rest-frame K-band luminosity function (LF) of galaxies from $z = 0$ up to $z = 4$, Domínguez et al. (2011) were able to model the EBL without any assumptions for the LF. Helgason & Kashlinsky (2012); Stecker et al. (2012) constructed evolving EBL models in a relatively robust way by utilizing multiwavelength photometric survey data.

Secondly, in forward evolution models, the basis is a description for the cosmic star formation history (CSFH), over which models for the spectral energy distribution (SED) of the stellar population are convolved to obtain the evolving EBL (e.g. Kneiske et al. 2004; Finke et al. 2010). However, such models cannot follow the detailed evolution of key physical quantities such as the metallicity and dust content, which can significantly affect the spectral shape of the EBL. Furthermore, although most forward evolution models employ the CSFH of Hopkins & Beacom (2006), it is known that this CSFH model overproduces the stellar mass density (Fardal et al. 2007; Choi & Nagamine 2012), and is also inconsistent with the observed rate of core-collapse supernovae (Horiuchi et al. 2011). Recent studies by Kobayashi et al. (2013) show that Hopkins (2004); Hopkins & Beacom (2006) may have overestimated the CSFH at $z > 1$, arising from over-correction for dust obscuration effects and in conversion from luminosity to star formation rate.

Finally, rooted in the modern cosmological framework of large-scale structure formation driven by cold dark matter, semi-analytical models of hierarchical galaxy formation account for the merging history of dark matter halos as well as the physical evolution of the baryonic component, including the effects of gas cooling, star formation, metal enrichment, feedback heating, etc. (Primack et al. 2005; Gilmore et al. 2009; Younger & Hopkins 2011; Gilmore et al. 2012b). Such models successfully reproduce various observed properties of galaxies from the local Universe up to $z \sim 6$ (see e.g., Kauffmann et al. 1993; Cole et al. 1994; Nagashima et al. 1999; Somerville & Primack 1999; Nagashima & Yoshii 2004; Baugh et al. 2005; Nagashima et al. 2005; Kobayashi et al. 2007, 2010; Somerville et al. 2012). At present, semi-analytical models can be considered the most detailed and well-developed models for the EBL over a wide range of redshifts.

A subject that has yet to be fully explored in the context of

the EBL and gamma-ray absorption is the epoch of cosmic reionization above $z \sim 6$. Measurements of NIR absorption troughs in the spectra of high- z quasars, together with those of anisotropies in the polarization of the cosmic microwave background (CMB), prove that the majority of intergalactic hydrogen in the Universe has been reionized somewhere between $z \sim 30$ and $z \sim 6$ (see e.g. Robertson et al. 2010). Although the most widely suspected source of reionization is UV photons emitted by early generations of massive stars, the observational constraints are still very limited, so that the actual sources, history and topology of cosmic reionization remain largely unknown. A closely related topic is the possible existence and formation history of Population III (Pop-III) stars, very massive stars that are expected to originate in nearly metal-free conditions, particularly for the very first generation of stars appearing in the Universe, and their potential role in cosmic reionization (see e.g. Bromm & Yoshida 2011; Glover 2012, and references therein).

Since the current observational constraints on reionization mostly concern the neutral or ionized intergalactic gas, it would be very valuable and complementary to obtain independent information on the evolving, UV intergalactic radiation field itself. A unique and promising approach may be offered by the effects of gamma-ray absorption in-situ in high-energy sources at $z > 6$. UV radiation fields with sufficient intensities to cause cosmic reionization may induce significant gamma-ray absorption at observer energies above a few tens of GeV (Oh 2001; Inoue et al. 2010a). Based on a semi-analytical model of galaxy formation that includes Pop-III stars and reproduces a variety of reionization-related observations (Choudhury & Ferrara 2006; Choudhury 2009), the recent study by Inoue et al. (2010a) suggested that appreciable attenuation may be expected above $\sim 12 \text{ GeV}$ at $z \sim 5$ and down to $\sim 6\text{--}8 \text{ GeV}$ at $z \gtrsim 8\text{--}10$, mainly caused by Pop-II stars at these epochs. However, the relative contribution of Pop-III stars was found to be difficult to discern observationally. On the other hand, without addressing the implications for reionization, some studies have concentrated on the prospects for constraining Pop-III star formation through gamma-ray absorption in objects at lower redshifts (e.g. Gilmore 2012).

The *Fermi* gamma-ray space telescope (Atwood et al. 2009, *Fermi*) may eventually detect blazars at $z > 6$ (Inoue et al. 2011), and the Cherenkov Telescope Array (Actis et al. 2011, CTA) may possibly do the same for gamma-ray bursts (GRBs) (Inoue et al. 2013). Therefore a deeper investigation into the above issues is worthwhile and timely. The above studies (Oh 2001; Inoue et al. 2010a; Gilmore 2012) have not accounted consistently for the EBL resulting from galaxy formation at lower redshifts. For example, the model of Inoue et al. (2010a) was optimized to describe the reionization epoch and did not include the contribution from Pop-I stars or dust, and thus could only evaluate the gamma-ray opacity above $z = 4$.

In this paper, we present a new study of the EBL and consequent gamma-ray opacity, covering the entire redshift range from $z = 0$ up to $z = 10$ within a consistent framework, accounting for the process of cosmic reionization, and including Pop-III stars in a simplified way. As a baseline model, we adopt the Mitaka model¹ of semi-analytical galaxy formation (Nagashima & Yoshii 2004). The model can reproduce various observed properties of galaxies such as their lu-

¹ Named after the city of Mitaka where the model was mainly developed at the National Astronomical Observatory of Japan.

minosity function (LF), luminosity density (LD), and stellar mass density (Nagashima & Yoshii 2004), as well as the LFs of high-redshift Lyman-break galaxies (LBGs) and Lyman- α emitters (LAEs) up to $z \sim 6$ (Kobayashi et al. 2007, 2010). As regards Pop-III stars, in view of the presently large theoretical uncertainties on their formation efficiency, metal production, conditions for transition to Pop-II star formation, etc., we choose not to fully incorporate them into our semi-analytical scheme. Instead, their formation history is characterized in a simple, parameterized way, which we constrain by modeling the cosmic reionization process and comparing with available observations, particularly the Thomson scattering optical depth measured by the Wilkinson Microwave Anisotropy Probe (*WMAP*).

We introduce our semi-analytical model in §2. Cosmic reionization is modeled and compared with observations in §3. §4 presents the results of our EBL models. The consequent gamma-ray opacity and comparison with current gamma-ray observations are described in §5. We conclude in §6. Throughout this paper, we adopt the standard cosmological parameters of $(h, \Omega_M, \Omega_\Lambda) = (0.7, 0.3, 0.7)$, and a Salpeter initial mass function (IMF; Salpeter 1955) within a mass range of $0.1 - 60 M_\odot$.

2. SEMI-ANALYTICAL GALAXY FORMATION MODEL

In the framework of the Mitaka semi-analytical model of galaxy formation, we follow the merger history of dark matter halos and the evolution of baryonic components. The evolution of the baryons within halos is modeled with physically motivated, phenomenological prescriptions for radiative cooling, star formation, supernova feedback, chemical enrichment, and galaxy merging. We can compute a variety of physical and observational quantities for individual galaxies as well as the global average over the Universe at any redshift, such as the CSFH, and LFs and dust content of galaxies. A mock catalog of galaxies can be generated that can be compared with different observations. More details of the Mitaka model are described in Nagashima & Yoshii (2004); Kobayashi et al. (2007, 2010). Several free parameters in the prescriptions for baryons are fixed so that they fit a number of observed properties of local galaxies, such as their B-band and K-band LFs, neutral gas fraction, and gas mass-to-luminosity ratio as a function of B-band luminosity (Nagashima & Yoshii 2004). For simplicity and consistency, we keep these parameters unchanged throughout this paper.

2.1. Cosmic Star Formation History

Fig. 1 shows the CSFH expected in the Mitaka model over $z = 0 - 18$ in different ranges of metallicity. Pop-III stars are expected to form from gas with metallicity below a critical value, such that the gas can only cool rather inefficiently through rotational transitions of molecular hydrogen, which leads to fragmentation into relatively massive protostellar clouds, and ultimately the formation of very massive stars. Once the metallicity exceeds this value, the gas can cool more efficiently via metal emission lines, and a transition to the formation of less massive, Population II (Pop-II) stars is thought to take place (e.g. Mackey et al. 2003; Bromm & Loeb 2003; Yoshida et al. 2004). However, the exact value of this critical metallicity has been debated, ranging from $Z = 10^{-6} Z_\odot = 10^{-7.7}$ (Schneider et al. 2006) to $Z =$

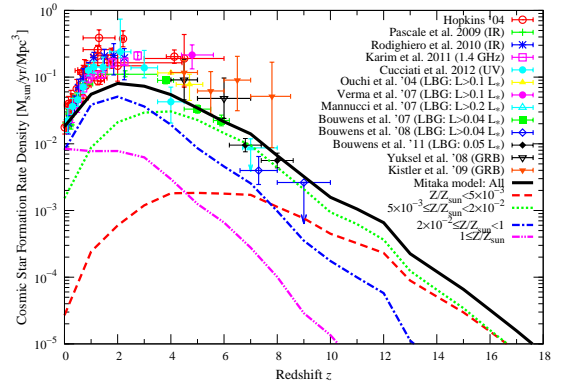


FIG. 1.— Cosmic star formation history. Solid curve shows the total in the baseline Mitaka model, while the dashed, dotted, dot-dashed and double-dot-dashed curves show the fractional contributions from stars with metallicity $Z/Z_\odot < 5 \times 10^{-3}$, $5 \times 10^{-3} \leq Z/Z_\odot < 2 \times 10^{-2}$, $2 \times 10^{-2} \leq Z/Z_\odot < 1$, and $Z/Z_\odot \geq 1$, respectively. We also plot the observational data compiled by Hopkins (2004), that deduced from LBGs (Ouchi et al. 2004; Bouwens et al. 2007; Mannucci et al. 2007; Verma et al. 2007; Bouwens et al. 2008), and that inferred from GRBs (Yüksel et al. 2008; Kistler et al. 2009). For the LBG sample, limiting luminosities adopted by each author are indicated in the corresponding legend in term of the characteristic luminosity L_* of the luminosity function.

$10^{-2} Z_\odot = 10^{-3.7}$ (Aykutalp & Spaans 2011)². In this paper, we consider stars with metallicity $Z < 10^{-4} = 5 \times 10^{-3} Z_\odot$ to correspond to Pop-III stars. We adopt a Salpeter IMF in the mass range of $0.1 - 60 M_\odot$ for all types of stars. Recent radiation-hydrodynamics simulations of Pop-III star formation suggest that their typical masses may be limited to $\lesssim 40 M_\odot$ due to radiative feedback effects (Hosokawa et al. 2011), which would be in accord with our choice of the the maximum mass for Pop-III stars.

We also plot the data compiled by Hopkins (2004); Pascale et al. (2009); Rodighiero et al. (2010); Karim et al. (2011); Cucciati et al. (2012), that deduced from LBGs, (Ouchi et al. 2004; Bouwens et al. 2007; Mannucci et al. 2007; Verma et al. 2007; Bouwens et al. 2008, 2011b), and that inferred from GRBs (Yüksel et al. 2008; Kistler et al. 2009). Above $z > 4$, each LBG data point is obtained by integrating its LF down to a certain limiting luminosity which is parameterized by the characteristic luminosity L_* of the LF, whose choice often differ among authors. Our model shows the star formation in all galaxies, down to the faintest luminosities.

There is an apparent discrepancy between our model and the observed CSFH data at $1 < z < 5$. In our semi-analytical model, we directly estimate the star formation rate for each galaxy and evaluate the CSFH by integrating over all galaxies. The CSFH data points are converted from the observed galaxy LFs and involve uncertainties in the faint-end slope of the LF, dust obscuration correction from UV data, contamination from old stellar populations to the IR luminosity, total IR luminosity modeling, and a conversion factor from luminosity to star formation rate. For the CSFH parameterizations of Hopkins (2004) and Hopkins & Beacom (2006), there are inconsistencies with other observational information such as the stellar mass density (e.g. Choi & Nagamine 2012), core collapse supernovae rate (Horiuchi et al. 2011) and con-

² We adopt $Z_\odot \simeq 0.02$ (Anders & Grevesse 1989; Grevesse & Sauval 1998), although an updated value of $Z_\odot \simeq 0.0134$ has been given by Asplund et al. (2009).

straints from gamma-ray observations (Rau & Meyer 2012). Recently, Kobayashi et al. (2013) have shown that this discrepancy arises from overcorrection in dust obscuration and star formation rate conversion, which leads to a factor of $\sim 2-3$ overestimation of the CSFH (Kobayashi et al. 2013). The discrepancy does not adversely affect our results, since our model can reproduce various other observed properties of galaxies. The comparison of the CSFH correction methods between Hopkins (2004) and Kobayashi et al. (2013) is discussed in Appendix A.

2.2. Stellar and Dust Emission

The cosmic emissivity due to stellar and reprocessed dust emission at a given frequency ν and redshift z is given by the sum of their respective emissivities $j_{\text{star}}(\nu, z)$ and $j_{\text{dust}}(\nu, z)$,

$$j(\nu, z) = j_{\text{star}}(\nu, z) + j_{\text{dust}}(\nu, z). \quad (2)$$

We calculate $j_{\text{star}}(\nu, z)$ from the CSFH using stellar population synthesis models that provide the SEDs as a function of metallicity and dust attenuation, namely the models of Bruzual & Charlot (2003) for $Z \geq 10^{-4}$ and Schaerer (2003) for $Z < 10^{-4}$ (Pop-III); note that the latter metallicity range is not covered by Bruzual & Charlot (2003). We adopt the Salpeter IMF for the models with a correction for the IMF mass range used in our model. Thus,

$$j_{\text{star}}(\nu, z) = \int_z^\infty \left| \frac{dt}{dz'} \right| dz' \int_0^\infty dZ \int_0^\infty dA_V f_{\text{esc}} \dot{\rho}_{\text{star}}(z', Z, A_V) \times \varepsilon(\nu', z', z, Z) \exp[-\tau_{\text{ISM}}(\nu', A_V) \times \tau_{\text{IGM}}(\nu, z', z)], \quad (3)$$

where A_V is the interstellar dust attenuation strength in the V-band, $\dot{\rho}_{\text{star}}(z, Z, A_V)$ is the CSFH for stars with metallicity Z and dust attenuation A_V at redshift z in units of $M_\odot \text{ yr}^{-1} \text{ Mpc}^{-3}$, $\varepsilon(\nu, z', z, Z)$ is the intrinsic emissivity at frequency ν at z from stars with metallicity Z born at z' in units of $\text{erg s}^{-1} \text{ Hz}^{-1} M_\odot^{-1}$ given by stellar population synthesis models, and $\nu' = (1+z')\nu/(1+z)$. τ_{ISM} and τ_{IGM} are the attenuation opacities in the interstellar medium (ISM) and the intergalactic medium (IGM), respectively. We adopt the ISM dust attenuation law of Calzetti et al. (2000) and the IGM opacity of Yoshii & Peterson (1994). f_{esc} is the escape fraction of photons from galaxies with energy above the threshold for ionization of hydrogen, $E = 13.6 \text{ eV}$; non-ionizing photons with lower energies are assumed to escape freely.

Various observations have constrained the UV LD up to $z \sim 6$ (Wyder et al. 2005; Schiminovich et al. 2005; Dahlen et al. 2007; Bouwens et al. 2007; Reddy et al. 2008). Fig. 2 compares the UV LD from our model with the observed LD data at a rest-frame wavelength of 1500 \AA . All the data agree well with our semi-analytical model. Comparison with other kinds of data are shown in Nagashima & Yoshii (2004); Nagashima et al. (2005); Kobayashi et al. (2007, 2010).

Dust emits mid-IR (MIR; $5 \sim 30 \mu\text{m}$) and FIR ($\sim 30 \sim 1000 \mu\text{m}$) photons by reemitting the absorbed starlight. For dust emission, we also utilize a new implementation in the Mitaka model (see Makiya et al. in preparation, for details). We set the total dust emissivity $J_{\text{dust}}(z) = \int_0^\infty d\nu j_{\text{dust}}(\nu, z)$ to be equivalent to the total starlight energy absorbed by dust in the ISM,

$$J_{\text{dust}}(z) = \int d\nu \int_z^\infty \left| \frac{dt}{dz'} \right| dz' \int_0^\infty dZ \int_0^\infty dA_V \dot{\rho}_{\text{star}}(z', Z, A_V) \times \varepsilon(\nu', z', z, Z) \{1 - \exp[-\tau_{\text{ISM}}(\nu', A_V)]\}. \quad (4)$$

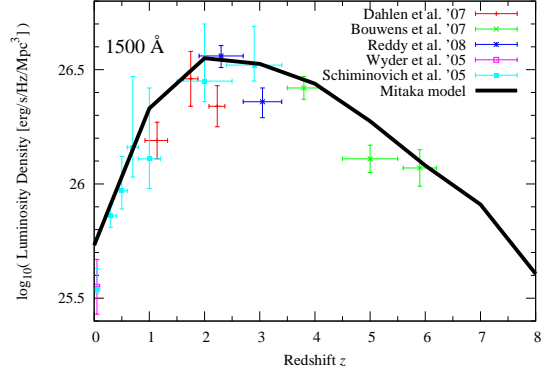


FIG. 2.— Luminosity density at rest-frame wavelength 1500 \AA . Solid curve is the result from the baseline Mitaka model. The observed data at various redshifts are also shown as indicated in the figure (Wyder et al. 2005; Schiminovich et al. 2005; Dahlen et al. 2007; Bouwens et al. 2007; Reddy et al. 2008).

To determine $j_{\text{dust}}(\nu, z)$, we utilize the model of dust emission SED by Dale & Helou (2002), where the IR SED shape is defined by the exponent α of their Eq. 1. We adopt $\alpha = 1.2$ for all galaxies in our model in order to reproduce the peak wavelength of the FIR EBL. Different α parameters result in different positions of the FIR peak wavelength.

Although our dust emissivity model can reproduce the local *Herschel* galaxy luminosity function (Vaccari et al. 2010), the redshift evolution of the IR luminosity function (e.g. Rodighiero et al. 2010) had yet to be reproduced (Makiya et al. in preparation). Thus, we predict an IR EBL at $z = 0$ that is lower than the current lower limits to the EBL by a factor of two. To remedy this, here we set the dust emissivity in our model to be three times more luminous than in the version of the Mitaka model by Makiya et al. (in preparation). Our model predictions in the MIR–FIR is therefore uncertain, while it should be more reliable in the UV–NIR band. We also note that the gamma-ray opacity due to the dust emission should be important only above several TeV in the local Universe (see Eq. 1).

3. COSMIC REIONIZATION HISTORY

After the epoch of cosmic recombination, the Universe entered the so-called dark ages, a period with no significant sources of radiation. As the initially small fluctuations in the matter density field grew by gravitational instability and collapsed to form dark matter halos, the baryons that fell into sufficiently massive halos are expected to have cooled efficiently to form the first stars and galaxies (Bromm & Yoshida 2011; Glover 2012). Such stars and galaxies should generate UV radiation that ionize their environments to create the first H II regions, which eventually grow and overlap to reionize the entire intergalactic medium. Observationally, cosmic reionization is known to have proceeded at least partially by $z \sim 10$ and been essentially completed by $z \sim 6$. However, the actual history, nature and sources of reionization are still largely unconstrained (see Barkana & Loeb 2001; Fan et al. 2006, for reviews). In this section, we discuss how we model the reionization history of the Universe with our Mitaka model.

3.1. Ionizing Photon Emission Rate

First we evaluate the emissivity of photons with energies greater than 13.6 eV that can ionize hydrogen atoms. A key

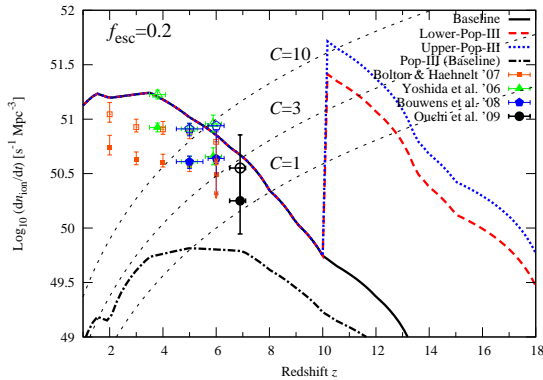


FIG. 3.— Ionizing photon emissivity per comoving Mpc^3 , dn_{ion}/dt , as a function of redshift. We set $f_{\text{esc}} = 0.2$ for all models and observed data. Solid, dashed, and dotted curves show the baseline, ($\xi = 1.0$ and $z_c = 0.0$), the lower-Pop-III, ($\xi = 50.0$ and $z_c = 10.0$), and the upper-Pop-III model ($\xi = 100.0$ and $z_c = 10.0$), respectively. Dot-dashed curve shows the ionizing photon emissivity from Pop-III population in the baseline model. The triangle, pentagon, and circle symbols show the data derived from the UV LFs of galaxies by Yoshida et al. (2006), Bouwens et al. (2008), and Ouchi et al. (2009), respectively. The data derived from the combination of hydrodynamical simulations and $\text{Ly}\alpha$ forest opacity (Bolton & Haehnelt 2007) are shown by square symbols. Filled and open symbols correspond to $\alpha_{\text{ion}} = 3$ and 1.5, respectively, for the spectral index of ionizing emission. Thin dashed lines plot the estimated ionizing photon emissivity that is required for maintaining the ionization of hydrogen in the IGM (Madau et al. 1999) for clumping factors of $C = 1, 3$, and 10, from bottom to top.

uncertainty is the escape fraction f_{esc} of ionizing photons from galaxies, which we assume here to be a constant value of 0.2 at all redshifts. This is motivated by the numerical simulations of Yajima et al. (2009, 2011), although they also showed that f_{esc} can depend on halo mass. Observationally, $f_{\text{esc}} \simeq 0.05$ is found in LBGs at $z \sim 3$ (Shapley et al. 2006; Iwata et al. 2009), but values at $z \geq 4$ have not been determined yet. Ono et al. (2010) have set upper limits of $f_{\text{esc}} \lesssim 0.6$ at $z = 5.7$ and $f_{\text{esc}} \lesssim 0.9$ at $z = 6.6$ for LAEs.

Fig. 3 shows the ionizing photon emissivity dn_{ion}/dt in units of $\text{s}^{-1} \text{Mpc}^{-3}$, compared with various observations. We set $f_{\text{esc}} = 0.2$ for interpretation of all the observed data as well. The observed ionizing emissivities were derived by Ouchi et al. (2009) from galaxy UV LFs at $z = 4 - 7$ (Yoshida et al. 2006; Bouwens et al. 2008; Ouchi et al. 2009, filled symbols in Fig. 3). The conversion from LF to ionizing photon emissivity is based on Eq. 5 in Ouchi et al. (2009), where continuous star formation history is assumed for all galaxies. The data are integrated down to $L = 0$. We also show the ionizing photon rate inferred from the $\text{Ly}\alpha$ forest by combining hydrodynamical simulations with measurements of the $\text{Ly}\alpha$ opacity of the IGM (Bolton & Haehnelt 2007, open symbols in Fig. 3).

As shown later, the baseline Mitaka model does not produce enough ionizing photons to account for the Thomson scattering optical depth measured by *WMAP*, although it can reionize the Universe sufficiently at $z \lesssim 8$. In order to achieve consistency with observations, we extend the baseline model by considering an additional potential contribution of ionizing photons from Pop-III stars in a simplified way. Although ideally one would like to incorporate Pop-III stars self-consistently into our semi-analytic scheme, this is currently precluded by very large uncertainties in their formation efficiency, metal yield, etc. Instead we introduce two new parameters and simply enhance the total ionizing photon emissivity

of the baseline Mitaka model by a constant factor ξ above a critical redshift z_c , and attribute such an additional component to Pop-III stars. An alternative procedure might be to enhance the emissivity of only the stellar population with $Z < 10^{-4}$ in the baseline model (Figs. 1 and 3), but this will not be more satisfactory in any way as the actual evolution of the metallicity would be altered. Thus we choose to simply enhance the total ionizing emissivity. In Fig. 3, we show the cases with $(\xi, z_c) = (50.0, 10.0)$ and $(50.0, 10.0)$, referred to as the lower-Pop-III model and the upper-Pop-III model, respectively. Also shown is the contribution of stars with $Z < 10^{-4}$ in the baseline model with $(\xi, z_c) = (1.0, 0.0)$. The corresponding star formation rates of Pop III stars at $z = 10$ will be 4.5×10^{-4} , 4.4×10^{-2} , and $8.8 \times 10^{-2} \text{M}_{\odot} \text{Mpc}^{-3} \text{yr}^{-1}$ for the baseline, the lower-Pop-III, and the upper-Pop-III model, respectively.

Although the overall behavior of our ionizing photon emissivity at $2 < z < 7$ is similar to that derived from the observed data, we overpredict the ionizing photon emissivity by about a factor of 2. We note that the data points are very sensitive to the assumed spectral index of the ionizing emission α_{ion} (see Eq. 5 in Ouchi et al. 2009), which is set to be 3.0 for the data in Fig. 3 but is actually not well determined. If $\alpha_{\text{ion}} = 1.5$, it will double the data derived from the galaxy UV LF and the $\text{Ly}\alpha$ forest opacity, bringing it into closer agreement with the model.

Fig. 3 also shows dn_{ion}/dt that is required to balance the recombination of intergalactic hydrogen based on the formulation of Madau et al. (1999),

$$\frac{dn_{\text{ion}}}{dt} = \frac{n_{\text{H}}^0}{t_{\text{rec}}(z)} \simeq 10^{47.4} C(1+z)^3 [\text{s}^{-1} \text{Mpc}^{-3}] \quad (5)$$

where n_{H}^0 is the total number density of intergalactic hydrogen atoms (in both HI and HII phases), $t_{\text{rec}}(z)$ is the recombination time scale at z , and $C = \langle n_{\text{H}}^2 \rangle / \bar{n}_{\text{H}}^2$ is a time-dependent, volume-averaged clumping factor, for which the cases of $C = 1, 3$, and 10 are shown. Note that $C = 1$ corresponds to a uniform IGM. All our models have a sufficient budget of photons to ionize the Universe at $z \leq 7 - 8$. However, the baseline model can not do so above $z = 8$, in contradiction with *WMAP* observations that constrain the reionization redshift to be $z = 10.6 \pm 1.2$ if it was instantaneous (Komatsu et al. 2011). Even if reionization occurred gradually, more ionizing photons may actually be necessary above $z \sim 8$ than is implied by the estimates of Madau et al. (1999).

3.2. Probing the Cosmic Reionization History

Important observational indicators of the reionization history are the optical depth to electron scattering and the neutral fraction of intergalactic hydrogen. Following Barkana & Loeb (2001), we compute the reionization history of the Universe. The equation of ionization equilibrium in terms of the volume filling factor Q_{HII} of HII regions is given by

$$\frac{dQ_{\text{HII}}}{dt} = \frac{1}{n_{\text{H}}^0} \frac{dn_{\text{ion}}}{dt} - \alpha_{\text{B}} \frac{C}{a(t)^3} n_{\text{H}}^0 Q_{\text{HII}}, \quad (6)$$

where t is the cosmic time, $n_{\text{H}}^0 = X_{\text{H}} n_{\text{B}}^0$ is the present-day number density of hydrogen with n_{B}^0 as the present-day baryon number density and $X_{\text{H}} = 0.76$ as the mass fraction of hydrogen, dn_{ion}/dt is the production rate of ionizing photons (see Fig. 3), and $\alpha_{\text{B}} = 2.6 \times 10^{-13} \text{cm}^3 \text{s}^{-1}$ is the recombination rate of hydrogen at temperature $T = 10^4 \text{K}$. The recombina-

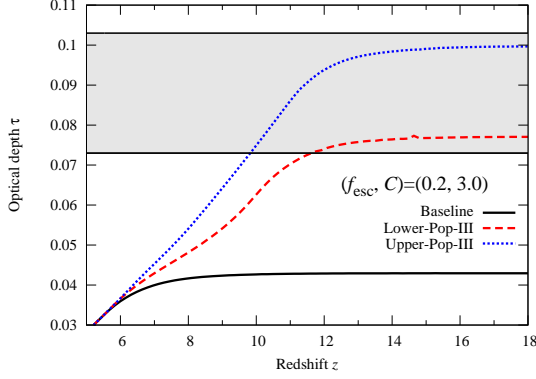


FIG. 4.— Thomson scattering optical depth of the IGM. We set $f_{\text{esc}} = 0.2$ and $C = 3.0$. Solid, dashed, and dotted curves correspond to the baseline, lower-Pop-III, and upper-Pop-III models, respectively. The shaded region shows the 7-year *WMAP* results with $1\text{-}\sigma$ errors, $\tau_e = 0.088 \pm 0.015$ (Komatsu et al. 2011).

tion time scale $t_{\text{rec}}(z)$ in Eq. 5 is given by $a(t)^3 / \alpha_B C n_H^0$, where $a(t)$ is the cosmic scale factor.

Assuming a constant clumping factor C , Equation 6 can be solved to give (see Barkana & Loeb 2001, for details)

$$Q_{\text{HII}}(z_0) = \int_{z_0}^{\infty} dz \left| \frac{dt}{dz} \right| \frac{1}{n_H^0} \frac{dn_{\text{ion}}}{dt} e^{F(z, z_0)}, \quad (7)$$

where dt/dz is calculated from the Friedmann equation in the standard, flat universe cosmology as

$$\frac{dt}{dz} = \frac{1}{(1+z)H_0 \sqrt{\Omega_M(1+z)^3 + \Omega_\Lambda}}. \quad (8)$$

Once Q_{HII} reaches 1, the IGM is fully ionized, and ionizing photons propagate freely in intergalactic space. The function $F(z, z_0)$ accounts for recombination and is given by

$$F(z, z_0) = -\frac{2}{3} \frac{\alpha_B n_H^0}{\sqrt{\Omega_M} H_0} C [f(z) - f(z_0)], \quad (9)$$

where $f(z)$ is defined as

$$f(z) = \sqrt{(1+z)^3 + \frac{1-\Omega_M}{\Omega_M}}. \quad (10)$$

For the purpose of calculating Q_{HII} , we set $C = 3.0$, motivated by the numerical simulations of Pawlik et al. (2009). We do not change C as a function of redshift. We also assume $Q_{\text{HeII}} = Q_{\text{HII}}$ for the volume filling factor of HeII regions and neglect the free electrons in HeIII regions for computing the optical depth to electron scattering. The number density of free electrons at z is then

$$\begin{aligned} n_e(z) &= \left(Q_{\text{HII}}(z) X_H + \frac{Q_{\text{HeII}}(1 - X_H)}{4} \right) n_B^0 (1+z)^3 \\ &= \frac{1+3X_H}{4} Q_{\text{HII}}(z) n_B^0 (1+z)^3. \end{aligned} \quad (11)$$

The optical depth to electron scattering is

$$\tau_e(z_0) = \int_0^{z_0} dz \frac{dl}{dz} \sigma_T n_e(z), \quad (12)$$

where σ_T is the Thomson cross section and dl/dz is the cosmological line element for a standard, flat universe cosmology

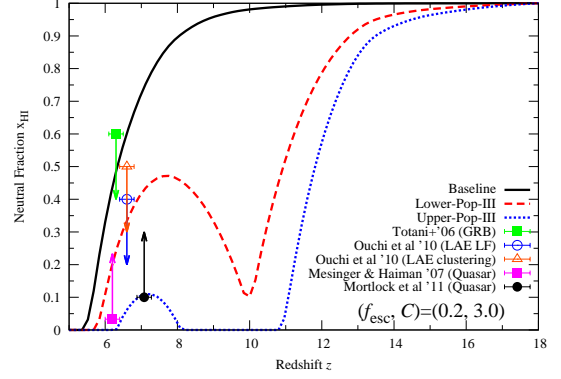


FIG. 5.— Neutral fraction of intergalactic hydrogen. We set $f_{\text{esc}} = 0.2$ and $C = 3.0$. Solid, dashed, and dotted curves correspond to the baseline, lower-Pop-III, and upper-Pop-III models, respectively. We also show observational constraints from quasars (Mesinger & Haiman 2007; Mortlock et al. 2011), a GRB (Totani et al. 2006), LAE LFs (Ouchi et al. 2010) and LAE clustering (Ouchi et al. 2010).

given by

$$\frac{dl}{dz} = c \frac{dt}{dz} = \frac{c}{(1+z)H_0 \sqrt{\Omega_M(1+z)^3 + \Omega_\Lambda}}. \quad (13)$$

Fig. 4 shows the Thomson scattering optical depth of the Universe, together with the range of $\tau_e = 0.088 \pm 0.015$ derived from the 7-year *WMAP* data (Komatsu et al. 2011). As mentioned above, the baseline model can not reproduce the *WMAP* data, despite managing to reionize the Universe at $z \lesssim 8$. The results of the lower-Pop-III and upper-Pop-III models are close to the lower and upper limits from *WMAP*, respectively, implying that 50-100 times more ionizing photons are necessary at $z \gtrsim 10$ than is conservatively expected from our semi-analytical galaxy formation model that successfully accounts for various observations at $z \lesssim 8$. The fact that the ionizing photon budget estimated from galaxy populations directly observed so far are insufficient to account for the *WMAP* τ_e is well documented (e.g. Stark et al. 2007; Chary 2008; Oesch et al. 2009; Ouchi et al. 2009; Pawlik et al. 2009; Bunker et al. 2010; Labbé et al. 2010; Robertson 2010; Bouwens et al. 2011a, 2012).

Fig. 5 shows $x_{\text{HI}} = 1 - Q_{\text{HII}}$, the neutral fraction of intergalactic hydrogen, compared with constraints from analysis of Gunn-Peterson (GP) troughs (Gunn & Peterson 1965) in the spectra of quasars (Mesinger & Haiman 2007; Mortlock et al. 2011) and a GRB (Totani et al. 2006). Also shown are constraints from LFs and clustering amplitudes of LAEs by (Ouchi et al. 2010). They derived $x_{\text{HI}} < 0.40$ at 1σ confidence level by comparing the observed LAE LFs at $z = 6.6$ with a theoretical model including Ly α transmission through the IGM, but the limit varies from 0.1 to 0.53 depending on the model (see §6.1.1. in Ouchi et al. 2010, for details). They also derived $x_{\text{HI}} \lesssim 0.50$ by comparing the angular correlation functions and bias of their LAE samples at $z = 6.6$ with the theoretical predictions of McQuinn et al. (2007) and Furlanetto et al. (2006).

We have not attempted a detailed comparison with GP measurements of quasars at $z \lesssim 6$ (e.g. Fan et al. 2006). Such effects depend rather sensitively on the detailed distribution of regions with low neutral gas density, which is not essential for our purposes of modeling the EBL.

Our baseline model that was inconsistent with *WMAP* is

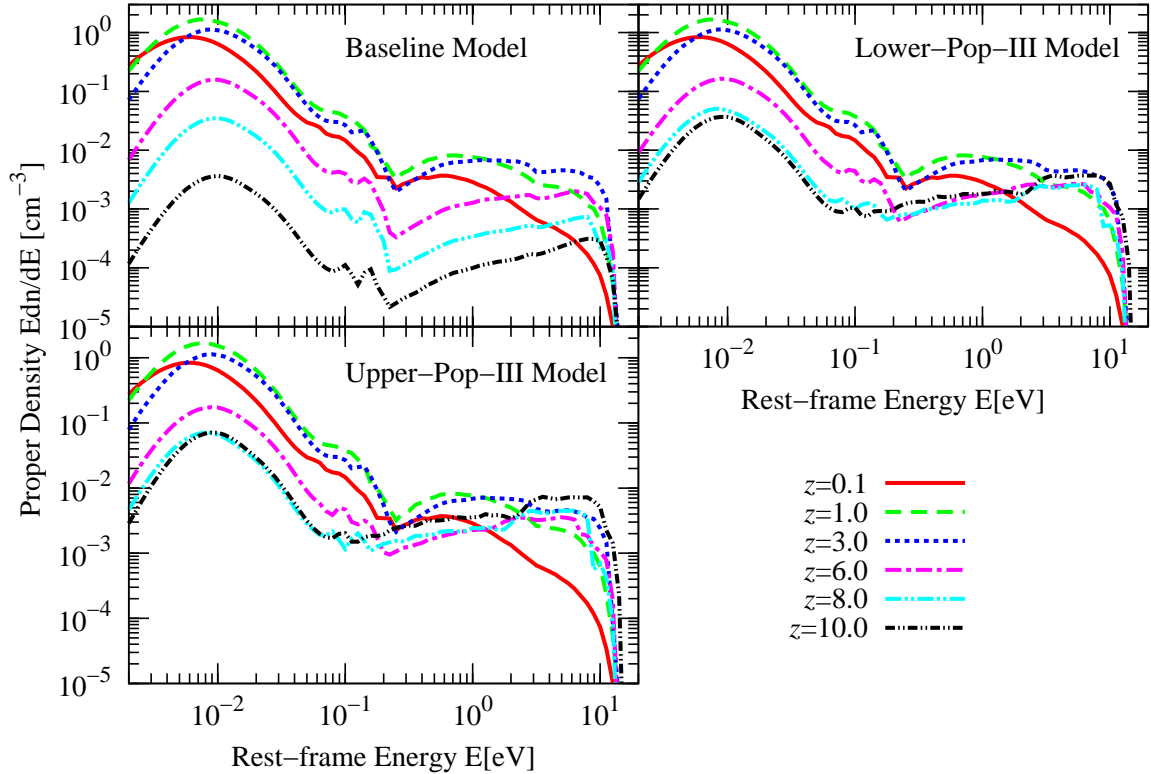


FIG. 6.— Proper volume photon number densities multiplied by the photon energy ϵ as a function of redshift. Top-left, top-right, and bottom-left panels correspond to the baseline, upper-Pop-III, and lower-Pop-III models, respectively. Solid, dashed, dotted, dot-dashed, double dot-dashed, and triple dot-dashed curves correspond to the proper photon density at $z = 0.1, 1.0, 3.0, 6.0, 8.0,$ and 10.0 , respectively.

also seen to contradict the LAE constraints on the neutral fraction (Ouchi et al. 2010) (which are rather model-dependent as discussed above). In contrast, both the lower-Pop-III and the upper-Pop-III models are generally consistent with the current observational limits, although the latter may be in marginal conflict with the GP constraints of Mesinger & Haiman (2007). Our simplifying assumption of a large enhancement of the ionizing photon emissivity only above $z = z_c$ in these two models leads to their nontrivial evolution of x_{HI} , with a dip at $z \sim 10$ due to reionization by Pop III stars alone, followed by a peak at $z \sim 7-8$ due to partial recombination after Pop III termination, and then finally complete reionization by Pop II stars (c.f. Cen (2003)). More realistic modeling with a smoother transition from Pop-III to Pop-II populations may make such features less pronounced.

Besides a large contribution from Pop-III stars, we note that various other aspects may be important in achieving sufficient ionizing photons at $z \gtrsim 8$ to account for the *WMAP* data (e.g. Haardt & Madau 2012; Kuhlen & Faucher-Giguère 2012). These include steepening of the faint-end slope of the LF (Bouwens et al. 2012), smaller clumping factor (Bolton & Haehnelt 2007; Pawlik et al. 2009), larger escape fraction (Yajima et al. 2011), harder initial mass function (McKee & Tan 2008), and X rays from accreting black holes (Ricotti & Ostriker 2004; Mirabel et al. 2011).

4. EXTRAGALACTIC BACKGROUND LIGHT

The background intensity $I(\nu_0, z_0)$ at redshift z_0 and frequency ν_0 is computed by integrating the radiation from all sources between $z = z_0$ and the maximum redshift of the

source distribution z_{max} (see e.g. Peacock 1999),

$$I(\nu_0, z_0) = \frac{1}{4\pi} \int_{z_0}^{z_{\text{max}}} dz \frac{dl}{dz} j(\nu, z), \quad (14)$$

where $j(\nu, z)$ is the comoving volume emissivity at redshift z and frequency $\nu = \nu_0(1+z)$, calculated by combining our CSFH and stellar population synthesis models. We set $z_{\text{max}} = 20$.

From Eq. 14, the specific radiation energy density (in units of $\text{erg s}^{-1} \text{cm}^{-3} \text{Hz}^{-1}$) in the proper volume is

$$\rho(\nu_0, z_0) = \frac{4\pi}{c} (1+z_0)^3 I(\nu_0, z_0) \quad (15)$$

The photon proper number density is

$$\frac{dn(\epsilon_0, z_0)}{d\epsilon_0} = \frac{\rho(\nu_0, z_0)}{\epsilon_0}, \quad (16)$$

where $\epsilon_0 = h_p \nu_0$ is the photon energy and h_p is the Planck constant.

Fig. 6 plots the proper photon number density for our models. The proper photon number density increases from $z = 10$ up to $z \sim 1-3$ where the CSFH reaches a peak and then decreases toward the local Universe. Once we increase the Pop-III component, the UV photon density at high redshifts becomes higher and comparable to that at $z = 1$. Although the IR photon density also increases, it is not as significant as the UV since there is little dust at high redshifts.

The EBL intensity at $z = 0$ for the baseline model is displayed in Fig. 7 as a function of wavelength λ . We also show

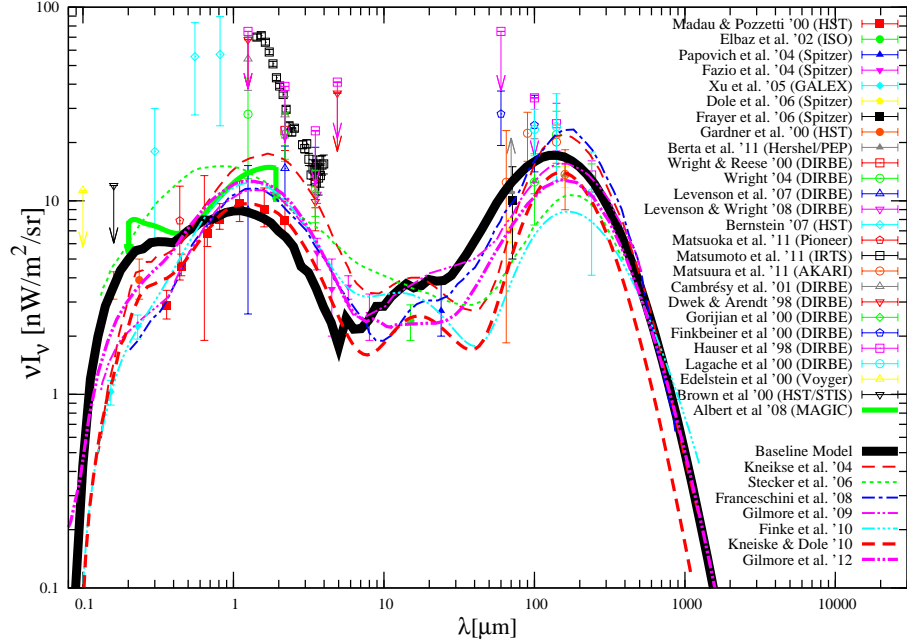


FIG. 7.— The EBL for the baseline model is shown by the solid curve. For comparison, the EBL models by Kneiske et al. (2004, thin dashed), Stecker et al. (2006, dotted), Franceschini et al. (2008, dot-dashed), Gilmore et al. (2009, thin double dot-dashed), Finke et al. (2010, triple dot-dashed), Kneiske & Dole (2010, thick dashed), and Gilmore et al. (2012b, thick double dot-dashed) are shown as indicated in the figure. The integrated brightness of galaxies (minimum EBL; filled symbols) and current measurements of the EBL (open symbols) are shown as indicated in the figure. References for the integrated brightness of galaxies are *HST* (Madau & Pozzetti 2000; Gardner et al. 2000), *ISO* (Elbaz et al. 2002), *Spitzer* (Papovich et al. 2004; Fazio et al. 2004; Dole et al. 2006; Frayer et al. 2006), *GALEX* (Xu et al. 2005), and *Herschel* (Berta et al. 2011). References for the current EBL measurements are *DIRBE* (Wright & Reese 2000; Wright 2004; Levenson et al. 2007; Levenson & Wright 2008; Cambrésy et al. 2001; Dwek & Arendt 1998; Gorjian et al. 2000; Finkbeiner et al. 2000; Hauser et al. 1998; Lagache et al. 2000), *HST* (Bernstein 2007; Brown et al. 2000), *Pioneer* (Matsuoka et al. 2011), *IRTS* (Matsumoto et al. 2005), *AKARI* (Matsuura et al. 2011), and *Voyager* (Edelstein et al. 2000). The upper limits from TeV gamma-ray observations by MAGIC (Albert et al. 2008) are also shown by the solid curve flanked by arrows.

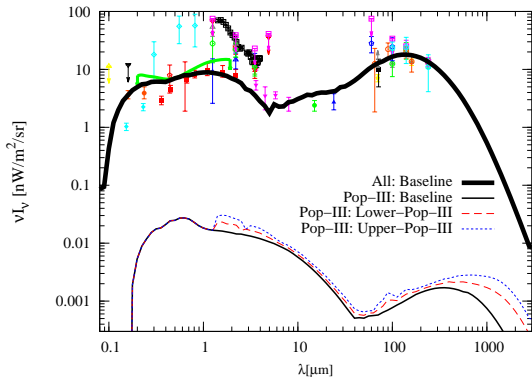


FIG. 8.— Same as Fig. 7, but showing the Pop-III contribution to the EBL. Thick solid curve shows the total EBL. Thin-solid, dashed, and dotted curve corresponds to the baseline, the upper-Pop-III and the lower-Pop-III model, respectively.

other theoretical models for comparison (Kneiske et al. 2004; Stecker et al. 2006; Franceschini et al. 2008; Gilmore et al. 2009; Finke et al. 2010; Kneiske & Dole 2010; Gilmore et al. 2012b), together with current measurements of the EBL and the integrated brightness of galaxies. Detailed predictions for the proper photon number density and the local EBL intensity is publicly available at our website³.

The overall shape of our EBL model is consistent with the observational data. Our model is in good agreement with the

observations by *Pioneer 10/11* (Matsuoka et al. 2011, open pentagon symbols in Fig. 7) which directly measured the EBL from outside the zodiacal region. It also does not violate the limits from gamma-ray observations (Aharonian et al. 2006a; Albert et al. 2008).

Compared to other models, we tend to predict more photons at $\lambda \leq 0.4 \mu\text{m}$ and less photons at $\lambda > 0.4 \mu\text{m}$. In the UV range, all other models except for Stecker et al. (2006) are consistent with the *GALEX* data (Xu et al. 2005), while ours are consistent with the *HST* data (Gardner et al. 2000). Both observational data points show the galaxy counts integrated down to zero luminosity. One reason for this difference may be in the treatment of dust obscuration. The Calzetti law (Calzetti et al. 2000) that we use was shown by Somerville et al. (2012) to result in more UV photons compared to the multi-dust component model adopted by Gilmore et al. (2012b); Somerville et al. (2012). We also note that the data points by Madau & Pozzetti (2000) are galaxy counts integrated down to the detection limit of the *HST*, implying a weaker lower-limit to the EBL.

At $0.4 \mu\text{m} < \lambda < 10 \mu\text{m}$, our model is in reasonably good agreement with Kneiske & Dole (2010) who provide lower-limits to the EBL. The CSFHs in our model and in Kneiske & Dole (2010) are a factor of two to three lower than that of Hopkins & Beacom (2006) that were used in most previous studies. We note that Kneiske & Dole (2010) only discussed the global average over the Universe and did not account for the distributions of metallicity and dust attenuation in different galaxies.

Fig. 8 shows the Pop-III contribution to the EBL in our

³ <http://www.slac.stanford.edu/~7eyinoue/Download.html>

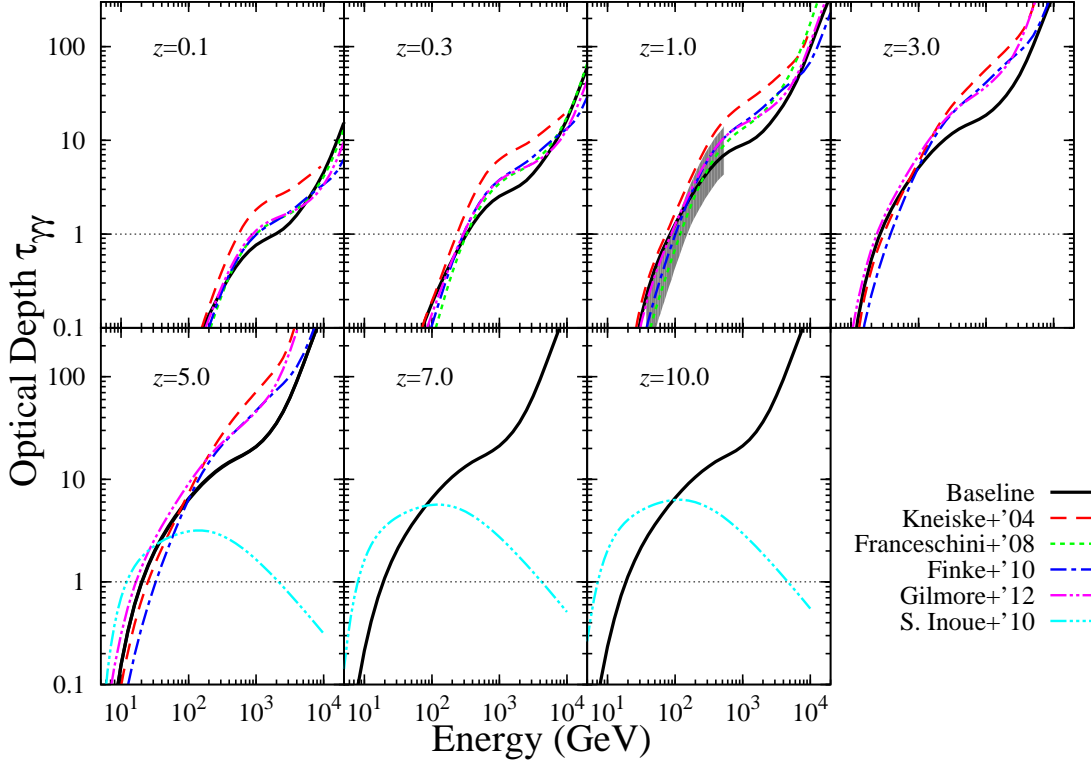


FIG. 9.— Optical depth to $\gamma\gamma$ interactions for observed gamma-ray energy E_γ and sources at $z = 0.1, 0.3, 1.0, 3.0, 5.0, 7.0,$ and 10.0 . Solid curves show our baseline model, which is nearly indistinguishable from our models including Pop-III stars. Dashed, dotted, dot-dashed, double dot-dashed, triple dot-dashed curves show the models by Kneiske et al. (2004) Franceschini et al. (2008), Finke et al. (2010), Gilmore et al. (2012b), and Inoue et al. (2010a), respectively. The shaded region represents the 95% confidence level measurement of the gamma-ray opacity by *Fermi* at $z \approx 1$ (Ackermann et al. 2012). The horizontal thin dotted line marks $\tau_{\gamma\gamma} = 1$.

models, which are all $\leq 0.03 \text{ nW m}^{-2} \text{ sr}^{-1}$ and less than 0.5% of the total NIR background radiation. It is far too low to explain the *IRTS* data (Matsumoto et al. 2005), even at the highest levels allowed by the reionization constraints (c.f. Fernandez et al. 2012). Moreover, even if the ionizing photons from Pop III stars that are absorbed inside galaxies are converted to Ly- α photons, the NIR flux will increase by only 15% in case B recombination. Therefore, the NIR background is unlikely to provide strong constraints on Pop III stars, at least in the framework of our model. Note that our Pop-III EBL spectrum shows two peaks, the one in the optical caused by the minor population at low z , and one in the NIR due to the redshifted, enhanced population at $z > z_c = 10$. For the upper-Pop-III model, the contribution from dust in the FIR can be a few percent of the total FIR EBL at $\lambda \gtrsim 1000 \mu\text{m}$.

5. GAMMA-RAY ATTENUATION

5.1. Gamma-ray Opacity

From the redshift-dependent intensity of the EBL as given in §4, we can compute the opacity for high-energy gamma rays to $\gamma\gamma$ pair production interactions. The cross section for this process is (Heitler 1954)

$$\sigma_{\gamma\gamma}(E_\gamma, \epsilon, \theta) = \frac{3\sigma_T}{16}(1-\beta^2) \times \left[2\beta(\beta^2-2) + (3-\beta^4) \ln\left(\frac{1+\beta}{1-\beta}\right) \right], \quad (17)$$

where ϵ is the energy of the background photon, E_γ is the energy of the propagating high energy photon, and β is

$$\beta \equiv \sqrt{1 - \frac{2m_e^2 c^4}{\epsilon E_\gamma (1 - \cos\theta)}}; \quad \mu \equiv \cos\theta. \quad (18)$$

where θ is the angle between the two colliding photons. The photon energy for which the cross section peaks is given by Eq. 1.

For a photon emitted by a source at redshift z_s and observed at $z = 0$ with energy E_γ , the contribution to the $\gamma\gamma$ optical depth between z_s and z_0 ($0 < z_0 < z_s$) is

$$\tau_{\gamma\gamma}(E_\gamma, z_0, z_s) = \int_{z_0}^{z_s} dz \int_{-1}^1 d\mu \int_{\epsilon_{\text{th}}}^{\infty} d\epsilon \frac{dl}{dz} \frac{1-\mu}{2} \times \frac{dn(\epsilon, z)}{d\epsilon} \sigma_{\gamma\gamma}(E_\gamma(1+z), \epsilon, \theta), \quad (19)$$

where ϵ_{th} is the pair production threshold energy,

$$\epsilon_{\text{th}} = \frac{2m_e^2 c^4}{E_\gamma(1+z)(1-\mu)}. \quad (20)$$

Fig. 9 shows the $\gamma\gamma$ optical depth as a function of the observed gamma-ray energy E_γ for sources at selected redshifts $z = 0 - 10$, compared with various previous models (Kneiske et al. 2004; Franceschini et al. 2008; Finke et al. 2010; Gilmore et al. 2012b; Inoue et al. 2010a). For all models, $z_0 = 0$ in Eq. 19, except for Inoue et al. (2010a) where

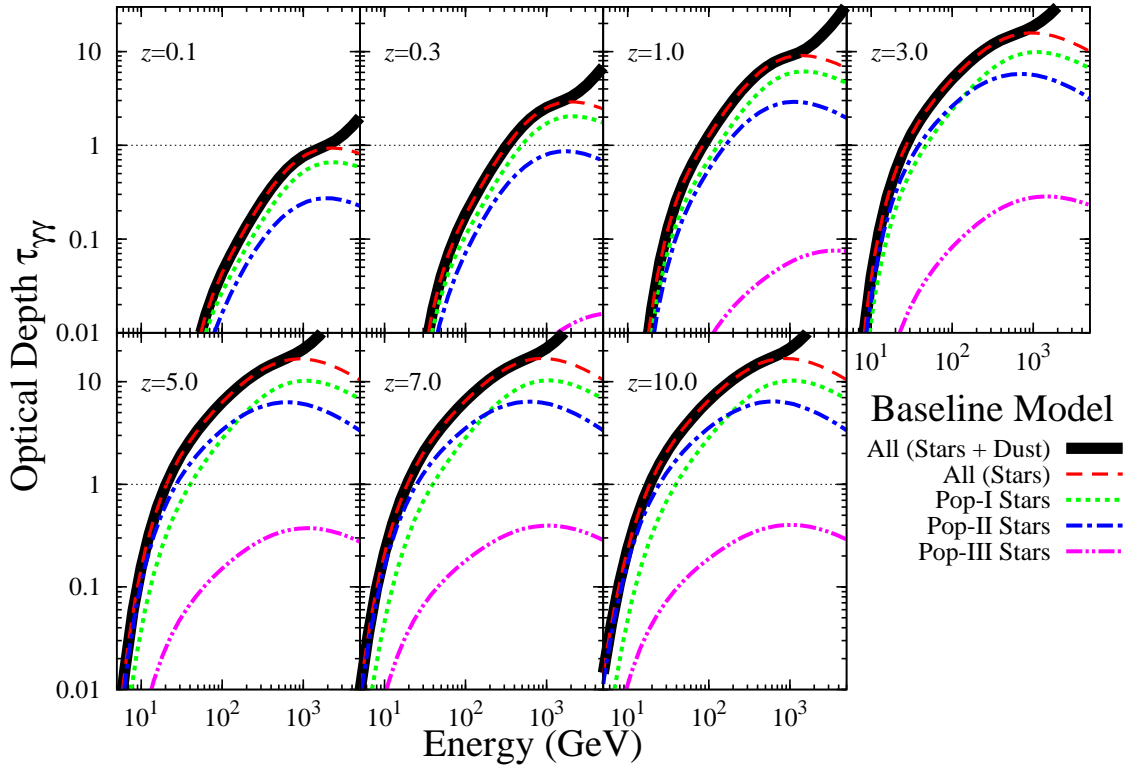


FIG. 10.— Same as Fig. 9, but separately for each stellar population. Solid, dashed, dotted, dot-dashed, and double dot-dashed curves show the contributions to the baseline model from all stars plus dust, all stars, Pop-I stars, Pop-II stars, and Pop-III stars, respectively. The contribution of Pop-III stars is small and does not appear in the panel for $z = 0.1$.

$z_0 = 4$, the minimum redshift in this model. For our model, only the baseline case is shown, since the Pop-III contribution turns out to be nearly indistinguishable (see below and §. 4). The detailed output for the $\gamma\gamma$ optical depth are publicly available at our website⁴. Absorption by the CMB photons is not included here. As described in §. 2.2, there are uncertainties in the redshift evolution of our dust emissivity model in the MIR–FIR, and consequently also in $\tau_{\gamma\gamma}$ above several TeV at $z = 0$. However, at these energies, the opacity due to stellar emission is already of order ~ 10 (See Fig. 10) and will likely mask such uncertainties.

Our model is consistent with the measurements of gamma-ray opacity by *Fermi* at $z \approx 1$ at the 95% confidence level (Ackermann et al. 2012). Although it is also generally consistent with previous models (Kneiske et al. 2004; Franceschini et al. 2008; Finke et al. 2010; Gilmore et al. 2012b) at $E_\gamma \lesssim 400/(1+z)$ GeV for $z \leq 5$, the opacity above $E_\gamma \sim 400/(1+z)$ GeV is a factor of ~ 2 lower. We recall that our local EBL is lower at $\lambda > 0.4 \mu\text{m}$ (Fig. 7), corresponding to $\gamma\gamma$ interactions preferentially with $\gtrsim 300$ GeV photons (Eq. 1).

For very high-redshift sources at $z \gtrsim 6$, we expect spectral attenuation above ~ 20 GeV. This is appreciably higher than in the model of Inoue et al. (2010a), who suggested ~ 12 GeV at $z \sim 5$ and ~ 6 – 8 GeV at $z \gtrsim 8$ – 10 . Their basis was the models of cosmic reionization by Choudhury & Ferrara (2006); Choudhury (2009), which included Pop III stars as well as QSOs and were developed to explain essentially all

observational constraints related to reionization, including τ_e from *WMAP* and x_{HI} from GP measurements. However, being optimized for the reionization epoch, they focused on $z \geq 4$ and did not account for Population-I stars with $Z > 0.02Z_\odot$ nor dust. While a thorough comparison between the two models is not feasible, the principal difference appears to be in the CSFH for Pop-II stars, which is a factor of ~ 3 – 10 higher at $z \gtrsim 6$ in Inoue et al. (2010a) compared to our baseline model here. This demonstrates that such differences in the CSFHs can be clearly distinguishable through future gamma-ray observations.

The highest redshifts of high-energy gamma-ray sources known so far are $z \sim 3$ for blazars and $z = 4.35$ for GRBs. Based on a model for the gamma-ray luminosity function of blazars, Inoue et al. (2011) proposed that *Fermi* may eventually detect blazars up to $z \sim 6$. GRBs are known to occur at $z > 6$ (Kawai et al. 2006; Greiner et al. 2009), at least up to $z \sim 8.2$ (Tanvir et al. 2009; Salvaterra et al. 2009), and probably out to the epoch of first star formation in the Universe (Bromm & Loeb 2006). If a bright burst similar to GRB 080916C (Abdo et al. 2009) occurs at such redshifts, CTA may be able to measure its spectrum up to $z \sim 7$ – 10 (Inoue et al. 2013) (and possibly even higher, see e.g. Toma et al. (2011)), offering a unique probe of the EBL during cosmic reionization.

Fig. 10 shows the $\gamma\gamma$ opacity due to each stellar population separately for the baseline model: Pop-I stars ($10^{-2.5} \leq Z$), Pop-II stars ($10^{-4} \leq Z < 10^{-2.5}$), and Pop-III stars ($Z < 10^{-4}$). Here we have chosen the dividing metallicity between Pop-II halo stars and Pop-I disk stars

⁴<http://www.slac.stanford.edu/~7eyinoue/Download.html>

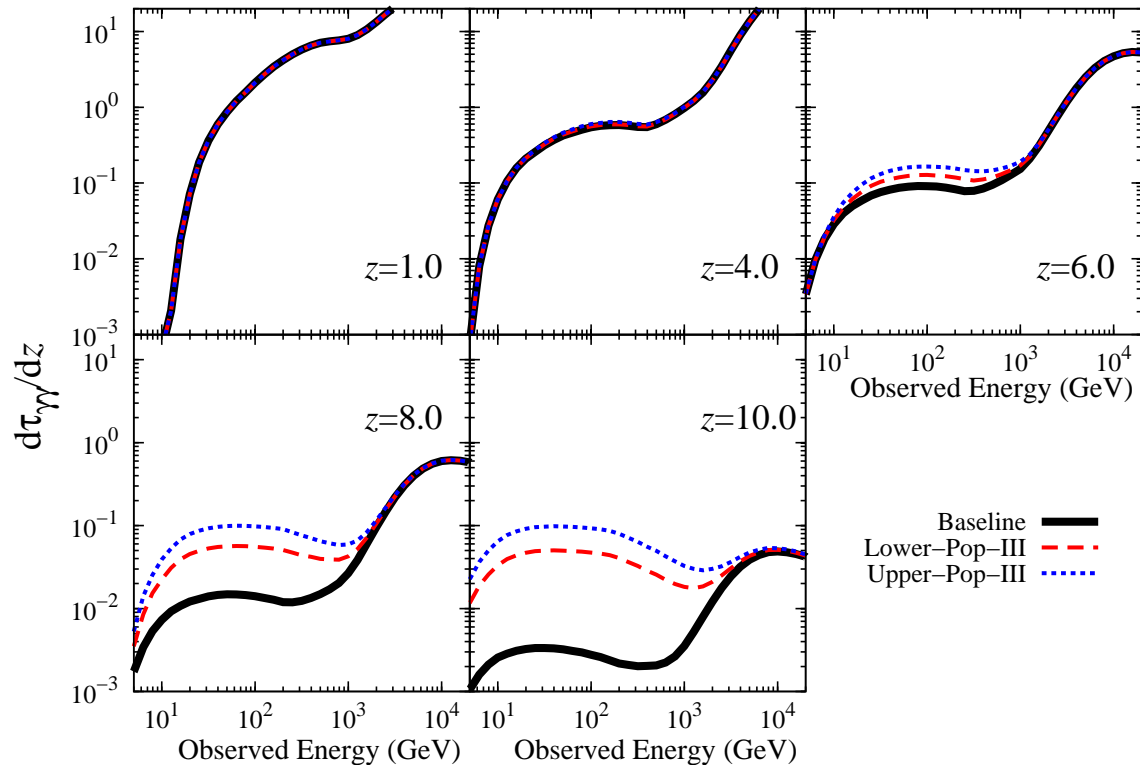


FIG. 11.— Differential $\gamma\gamma$ optical depth $d\tau_{\gamma\gamma}/dz$ with respect to redshift z for observed gamma-ray energy E_γ and sources at $z = 1.0, 4.0, 6.0, 8.0,$ and 10.0 . Solid, dashed, and dotted curves show the baseline, lower-Pop-III, and upper-Pop-III models, respectively.

to be $Z = 10^{-2.5}$, as the distinction between the two populations is known to occur at $[\text{Fe}/\text{H}] \simeq -1$, corresponding to $Z \simeq 10^{-2.7} - 10^{-2.3}$ (Wheeler et al. 1989; McWilliam 1997; Prochaska et al. 2000). Although the gamma-ray attenuation signature of Pop-III stars seems difficult to discern, that due to Population II stars should be observable in future observations of high- z gamma-ray sources and will provide a valuable probe of the evolving UV EBL in the cosmic reionization epoch. The detection of even one photon from such redshifts will impose useful limits on cosmic reionization models as well as Pop III stars.

Fig. 11 shows the differential contributions to the $\gamma\gamma$ optical depth $d\tau_{\gamma\gamma}/dz$ with respect to redshift in our models. Since the Pop-III component is enhanced only at $z > 10$, its effect at $z \lesssim 6$ is insignificant, while at $z \gtrsim 6$, differences can be seen of $\sim 3\%$, $\sim 10\%$ and $\sim 20\%$ at 20 GeV relative to the baseline model at $z = 6, 8,$ and 10 , respectively. Discrimination between the models would be possible only if differences of $\sim 10\%$ in flux can be identified.

5.2. Comparison with Current GeV & TeV data

Gamma-ray astronomy has seen enormous progress during the last decade, led by new generation facilities such as *Fermi*, H.E.S.S., MAGIC, and VERITAS, among others. Further progress is anticipated in the near future with CTA. CTA is expected to detect > 100 blazars up to $z \sim 2.5$ (Inoue et al. 2010b; Inoue for the CTA Consortium 2011; Sol et al. in press). It is also expected to detect GRBs at a rate of order a few per year, possibly out to much higher redshifts (Kakuwa et al. 2012; Gilmore et al. 2012a; Inoue et al. 2013). Such observations will allow us to greatly clarify the

evolution of the EBL in the UV-NIR bands. Detailed observations of TeV blazars at low z will also be crucial for probing the FIR EBL, which would not be possible with high- z sources. Starburst galaxies have also been suggested as alternative targets for studying the FIR EBL (Dwek & Krennrich 2012), even though internal gamma-ray absorption may limit their usefulness (e.g. Inoue 2011b).

The gamma-ray horizon energy at which $\tau_{\gamma\gamma} = 1$ as a function of z , known as the Fazio–Stecker relation (Fazio & Stecker 1970), is shown in Fig. 12 in comparison with other models (Kneiske et al. 2004; Franceschini et al. 2008; Finke et al. 2010; Gilmore et al. 2012b; Inoue et al. 2010a). We also plot the maximum energies of photons detected from a sample of blazars (see Finke & Razzaque 2009, for a list and references) as well as GRB 080916C (Abdo et al. 2009). The inset in Fig. 12 is a blow up for $z = 5 - 10$ to emphasize the differences among our models with and without Pop-III stars.

The highest photon energies for many blazars lie in regions considerably above the $\tau_{\gamma\gamma} = 1$ curves for all EBL models, indicating that their spectra are likely to be highly attenuated. It is also clear that GRB 080916C provides an important constraint on the EBL at $z \sim 4$. Our model predicts that the Universe is transparent below 20 GeV even at $z > 4$.

Figs. 13 and 14 show the observed spectra of TeV blazars at $z \leq 0.15$ and $z > 0.15$, respectively, together with their intrinsic spectra before attenuation by the EBL, assuming our baseline model. If the TeV emission from these sources originate from electrons accelerated according to the simplest, test-particle theory of diffusive shock acceleration (Blandford & Eichler 1987), the hardest spectrum is expected

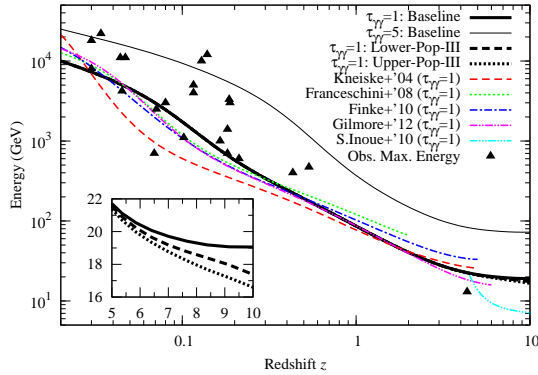


FIG. 12.— Gamma-ray horizon energy where $\tau_{\gamma\gamma} = 1$. The baseline, lower-Pop-III, and upper-Pop-III models are shown by the thick solid, thick dashed, and thick dotted curves, respectively. Dashed, dotted, dot-dashed, double dot-dashed, triple dot-dashed curves represent the models by Kneiske et al. (2004) Franceschini et al. (2008), Finke et al. (2010), Gilmore et al. (2012b), and Inoue et al. (2010a), respectively. The thin solid curve shows the case of $\tau_{\gamma\gamma} = 5$ for the baseline model. The filled data points are the observed maximum energies of photons from a sample of blazars (Finke & Razzaque 2009) and GRB 080916 C (Abdo et al. 2009). Since other papers do not cover the opacity at $z = 0-10$, we do not show the opacity of each model at the outside of the redshift range of each paper. The small panel in the figure shows the gamma-ray opacity horizon at $z = 5-10$.

to be of photon index $\Gamma_{\text{int}} = 1.5$. Although the intrinsic spectra inferred here are generally consistent with $\Gamma_{\text{int}} \geq 1.5$, some sources such as 1ES 0229+20 and 1ES 1101-232 show evidence of harder spectra above several hundred GeV (see also Finke et al. 2010).

To explain such intrinsically hard spectra, some authors have recently suggested secondary cascade components generated by very high energy cosmic-rays or gamma-rays, which may also offer a probe of intergalactic magnetic fields (e.g. Essey & Kusenko 2010; Essey et al. 2011; Essey & Kusenko 2012; Murase et al. 2012; Aharonian et al. 2012). Others have proposed effects of time-dependence, stochastic acceleration or multiple emission components (Lefa et al. 2011b,a). Future CTA observations of these objects with high energy and time resolution will elucidate such issues.

The signature of EBL absorption has not been seen in the spectrum of the extragalactic gamma-ray background (EGB) above 100 GeV (Ackermann et al. 2011), even though it is naturally expected if its origin is cosmological (Inoue 2011a; Inoue & Ioka 2012). By considering the effects of cascade emission, Inoue & Ioka (2012) have recently shown that if the EGB at <100 GeV (Abdo et al. 2010b) is entirely composed of known types of sources whose spectra are well constrained by existing observations, the measured EGB at >100 GeV would be inconsistent with this hypothesis, even for a low EBL such as proposed here. Further detailed spectral studies of extragalactic gamma-ray sources are required to resolve this issue.

6. CONCLUSIONS

We have developed models for the EBL over the redshift range $z = 10$ to $z = 0$ on the basis of a semi-analytical model of

hierarchical galaxy formation, into which Pop-III stars were incorporated in a simplified fashion. Our baseline model is consistent with a wide variety of observational data for galaxies below $z \sim 6$ (Nagashima & Yoshii 2004; Kobayashi et al. 2007, 2010), and is also capable of reionizing the Universe by $z < 8$. However, in order to account for the Thomson scattering optical depth measured by *WMAP*, the ionizing photon emissivity is required to be 50-100 times higher at $z > 10$. This is line with recent observations of galaxy candidates at $z \sim 8$, as long as the contribution from faint galaxies below the sensitivity of current telescopes is not large (e.g. Bouwens et al. 2012). The “missing” ionizing photons may possibly be supplied by Pop-III stars forming predominantly at these epochs in sufficiently small galaxies.

The EBL intensity at $z = 0$ in our model is generally not far above the lower limits derived from galaxy counts. Our model is also in good agreement with the data from *Pioneer* (Matsuoka et al. 2011) directly measured from outside the zodiacal region. The Pop-III contribution to the NIR EBL is ≤ 0.03 nW m⁻² sr⁻¹, less than 0.5 % of the total in this band, even at the maximum level compatible with *WMAP* measurements. The putative NIR EBL excess (Matsumoto et al. 2005), which also conflicts with the upper limits from gamma-ray observations (Aharonian et al. 2006a), may have a zodiacal origin rather than Pop-III stars.

Up to $z \sim 3-5$, the $\gamma\gamma$ opacity in our model is comparable to that in the majority of previously published models (Kneiske et al. 2004; Franceschini et al. 2008; Finke et al. 2010; Gilmore et al. 2012b) below $E_\gamma \sim 400/(1+z)$ GeV, while it is a factor of ~ 2 lower above this energy. The Universe is predicted to be largely transparent below 20 GeV even at $z > 4$.

Estimates based on the observed gamma-ray luminosity function of blazars show that *Fermi* may detect blazars up to $z \sim 6$ (Inoue et al. 2011). CTA may possibly detect GRBs up to similar redshifts (Inoue et al. 2013). However, the contribution of Pop-III stars may be difficult to discern in the attenuated spectra of high-redshift gamma-ray sources, even at the highest levels allowed by the *WMAP* constraints. Nevertheless, the signature of Population II stars is expected to be observable in high- z gamma-ray sources, providing a unique and valuable probe of the evolving EBL in the rest-frame UV.

We thank the anonymous referee for useful comments and suggestions. We also thank Floyd Stecker and Alberto Dominguez for helpful comments and Tirth Roy Choudhury for providing numerical data from his model. YI acknowledges support by the Research Fellowship of the Japan Society for the Promotion of Science (JSPS). SI is supported by Grants-in-Aid Nos. 22540278 and 24340048 from MEXT of Japan.

REFERENCES

- Abdo, A. A. et al. 2009, *Science*, 323, 1688
 —. 2010a, *ApJ*, 723, 1082
 —. 2010b, *Physical Review Letters*, 104, 101101
 Abramowski, A. et al. 2012a, *A&A*, 538, A103
 —. 2012b, *A&A*, 542, A94
 —. 2013, *A&A*, 550, A4
 Acciari, V. et al. 2009a, *ApJ*, 690, L126
 Acciari, V. A. et al. 2008, *ApJ*, 684, L73
 —. 2009b, *ApJ*, 695, 1370
 —. 2010, *ApJ*, 715, L49

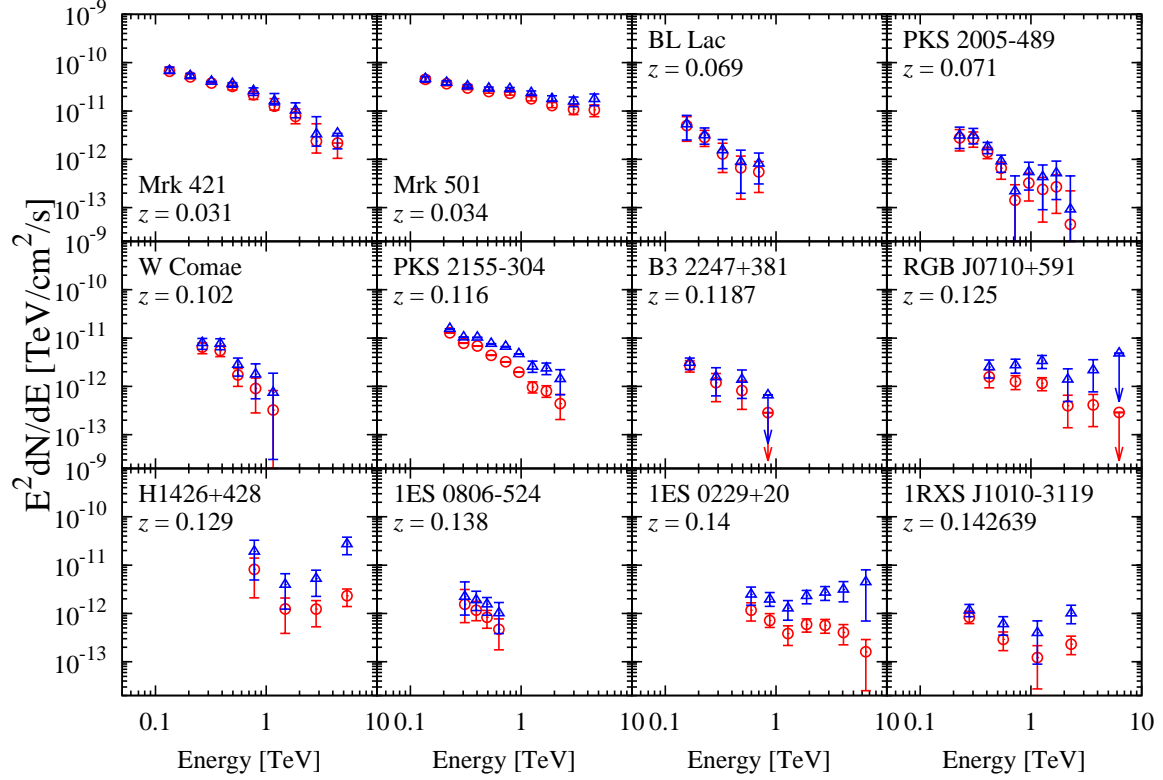


FIG. 13.— Spectra of TeV blazars at $z \leq 0.15$ as observed before EBL attenuation (circle) and inferred before EBL attenuation (triangle) with our baseline model. References for the data are Mrk 421 (Albert et al. 2007c), Mrk 501 (Albert et al. 2007d), BL Lac (Albert et al. 2007a), PKS 2005-489 (Aharonian et al. 2005a), W Comae (Acciari et al. 2008), PKS 2155-304 (Aharonian et al. 2005b), B3 2247+381 (Aleksić et al. 2012), RGB J0710+591 (Acciari et al. 2010), H 1426+428 (Aharonian et al. 2002), 1ES 0806-524 (Acciari et al. 2009a), 1ES 0229+200 (Aharonian et al. 2007c), 1RXS J1010-3119 (Abramowski et al. 2012b).

Ackermann, M. et al. 2011, *TeV Particle Astrophysics 2011*
— 2012, *Science*, 338, 1190
Actis, M. et al. 2011, *Experimental Astronomy*, 32, 193
Aharonian, F., Essey, W., Kusenko, A., & Prosekin, A. 2012, arXiv:1206.6715
Aharonian, F. et al. 2002, *A&A*, 384, L23
— 2005a, *A&A*, 436, L17
— 2005b, *A&A*, 442, 895
— 2006a, *Nature*, 440, 1018
— 2006b, *A&A*, 455, 461
— 2007a, *A&A*, 470, 475
— 2007b, *A&A*, 473, L25
— 2007c, *A&A*, 475, L9
Albert, J. et al. 2007a, *ApJ*, 666, L17
— 2007b, *ApJ*, 667, L21
— 2007c, *ApJ*, 663, 125
— 2007d, *ApJ*, 669, 862
— 2008, *Science*, 320, 1752
Aleksić, J. et al. 2011a, *ApJ*, 730, L8
— 2011b, *ApJ*, 726, 58
— 2012, *A&A*, 539, A118
Aliu, E. et al. 2011, *ApJ*, 742, 127
— 2012, *ApJ*, 750, 94
Anderhub, H. et al. 2009, *ApJ*, 704, L129
Anders, E. & Grevesse, N. 1989, *Geochim. Cosmochim. Acta*, 53, 197
Asplund, M., Grevesse, N., Sauval, A. J., & Scott, P. 2009, *ARA&A*, 47, 481
Atwood, W. B. et al. 2009, *ApJ*, 697, 1071
Aykatalp, A. & Spaans, M. 2011, *ApJ*, 737, 63
Barkana, R. & Loeb, A. 2001, *Phys. Rep.*, 349, 125
Baugh, C. M., Lacey, C. G., Frenk, C. S., Granato, G. L., Silva, L., Bressan, A., Benson, A. J., & Cole, S. 2005, *MNRAS*, 356, 1191
Bernstein, R. A. 2007, *ApJ*, 666, 663
Berta, S. et al. 2011, *A&A*, 532, A49
Blandford, R. & Eichler, D. 1987, *Phys. Rep.*, 154, 1
Bolton, J. S. & Haehnelt, M. G. 2007, *MNRAS*, 382, 325
Bouwens, R. J., Illingworth, G. D., Franx, M., & Ford, H. 2007, *ApJ*, 670, 928
— 2008, *ApJ*, 686, 230
Bouwens, R. J. et al. 2011a, *Nature*, 469, 504
— 2011b, *ApJ*, 737, 90

— 2012, *ApJ*, 752, L5
Bromm, V. & Loeb, A. 2003, *Nature*, 425, 812
— 2006, *ApJ*, 642, 382
Bromm, V. & Yoshida, N. 2011, *ARA&A*, 49, 373
Brown, T. M., Kimble, R. A., Ferguson, H. C., Gardner, J. P., Collins, N. R., & Hill, R. S. 2000, *AJ*, 120, 1153
Bruzual, G. & Charlot, S. 2003, *MNRAS*, 344, 1000
Bunker, A. J. et al. 2010, *MNRAS*, 409, 855
Calzetti, D., Armus, L., Bohlin, R. C., Kinney, A. L., Koornneef, J., & Storchi-Bergmann, T. 2000, *ApJ*, 533, 682
Cambrésy, L., Reach, W. T., Beichman, C. A., & Jarrett, T. H. 2001, *ApJ*, 555, 563
Cen, R. 2003, *ApJ*, 591, L5
Chary, R.-R. 2008, *ApJ*, 680, 32
Choi, J.-H. & Nagamine, K. 2012, *MNRAS*, 419, 1280
Choudhury, T. R. 2009, *Current Science*, 97, 841
Choudhury, T. R. & Ferrara, A. 2006, *MNRAS*, 371, L55
Cole, S., Aragon-Salamanca, A., Frenk, C. S., Navarro, J. F., & Zepf, S. E. 1994, *MNRAS*, 271, 781
Cucciati, O. et al. 2012, *A&A*, 539, A31
Dahlen, T., Mobasher, B., Dickinson, M., Ferguson, H. C., Giavalisco, M., Kretchmer, C., & Ravindranath, S. 2007, *ApJ*, 654, 172
Dale, D. A. & Helou, G. 2002, *ApJ*, 576, 159
Dole, H. et al. 2006, *A&A*, 451, 417
Domínguez, A. et al. 2011, *MNRAS*, 410, 2556
Dwek, E. & Arendt, R. G. 1998, *ApJ*, 508, L9
Dwek, E. & Krennrich, F. 2012, arXiv:1209.4661
Edelstein, J., Bowyer, S., & Lampton, M. 2000, *ApJ*, 539, 187
Elbaz, D., Cesarsky, C. J., Chanial, P., Aussel, H., Franceschini, A., Fadda, D., & Chary, R. R. 2002, *A&A*, 384, 848
Essey, W., Kalashev, O., Kusenko, A., & Beacom, J. F. 2011, *ApJ*, 731, 51
Essey, W. & Kusenko, A. 2010, *Astroparticle Physics*, 33, 81
— 2012, *ApJ*, 751, L11
Fan, X., Carilli, C. L., & Keating, B. 2006, *ARA&A*, 44, 415
Fardal, M. A., Katz, N., Weinberg, D. H., & Davé, R. 2007, *MNRAS*, 379, 985
Fazio, G. G. & Stecker, F. W. 1970, *Nature*, 226, 135
Fazio, G. G. et al. 2004, *ApJS*, 154, 39
Fernandez, E. R., Iliev, I. T., Komatsu, E., & Shapiro, P. R. 2012, *ApJ*, 750, 20

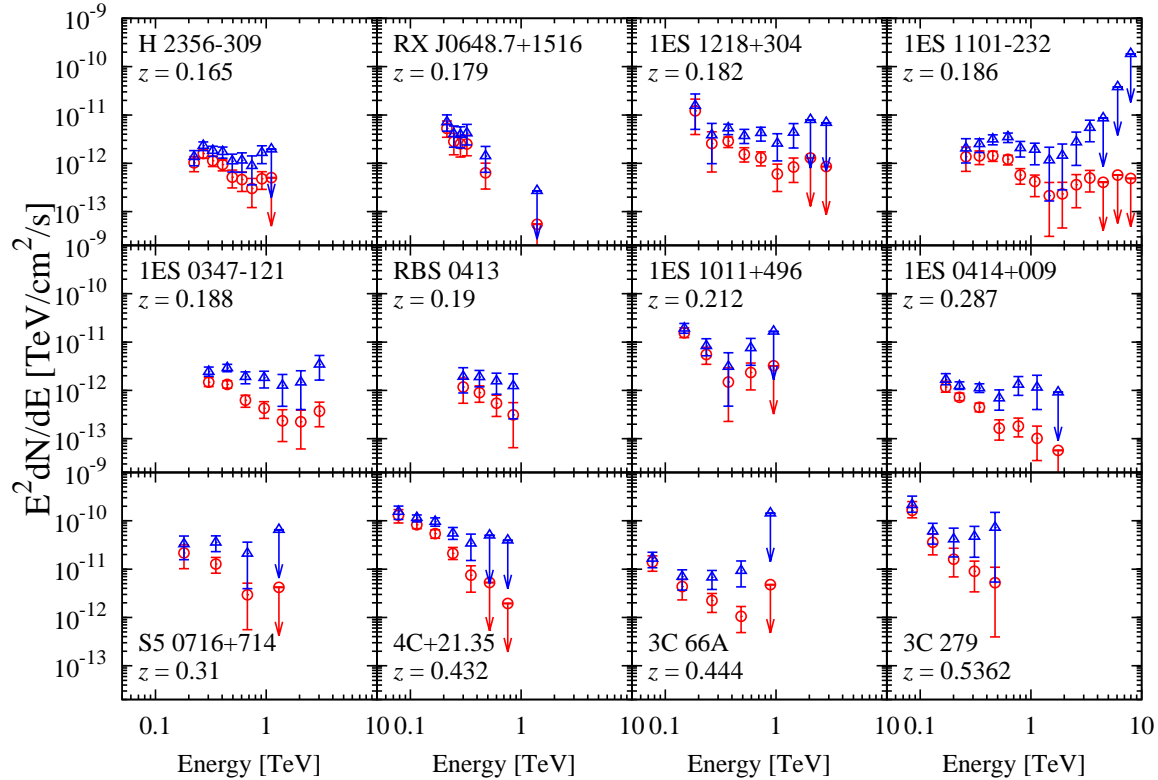


FIG. 14.— Same as Fig. 13, but for sources at $z > 0.15$. References for the data are H 2356-309 (Aharonian et al. 2006b), RX J0648.7+1516 (Aliu et al. 2011), 1ES 1218+304 (Acciari et al. 2009b), 1ES 1101-232 (Aharonian et al. 2007a), 1ES 0347-121 (Aharonian et al. 2007b), RBS 0413 (Aliu et al. 2012), 1ES 1011+496 (Albert et al. 2007b), 1ES 0414+009 (Abramowski et al. 2012a), S5 0716+714 (Anderhub et al. 2009), 4C+21.35 (Aleksić et al. 2011a), 3C 66A (Aleksić et al. 2011b), 3C 279 (Albert et al. 2008).

- Finkbeiner, D. P., Davis, M., & Schlegel, D. J. 2000, *ApJ*, 544, 81
 Finke, J. D. & Razzaque, S. 2009, *ApJ*, 698, 1761
 Finke, J. D., Razzaque, S., & Dermer, C. D. 2010, *ApJ*, 712, 238
 Franceschini, A., Rodighiero, G., & Vaccari, M. 2008, *A&A*, 487, 837
 Frayer, D. T. et al. 2006, *ApJ*, 647, L9
 Furlanetto, S. R., Zaldarriaga, M., & Hernquist, L. 2006, *MNRAS*, 365, 1012
 Gardner, J. P., Brown, T. M., & Ferguson, H. C. 2000, *ApJ*, 542, L79
 Giavalisco, M. et al. 2004, *ApJ*, 600, L103
 Gilmore, R. C. 2012, *MNRAS*, 420, 800
 Gilmore, R. C., Bouvier, A., Connaughton, V., Goldstein, A., Otte, N., Primack, J. R., & Williams, D. A. 2012a, *Experimental Astronomy*, 41
 Gilmore, R. C., Madau, P., Primack, J. R., Somerville, R. S., & Haardt, F. 2009, *MNRAS*, 399, 1694
 Gilmore, R. C., Somerville, R. S., Primack, J. R., & Domínguez, A. 2012b, *MNRAS*, 422, 3189
 Glover, S. C. O. 2012, *ArXiv e-prints*
 Gorjian, V., Wright, E. L., & Chary, R. R. 2000, *ApJ*, 536, 550
 Gould, R. J. & Schröder, G. 1966, *Physical Review Letters*, 16, 252
 Greiner, J. et al. 2009, *ApJ*, 693, 1610
 Grevesse, N. & Sauval, A. J. 1998, *Space Sci. Rev.*, 85, 161
 Gunn, J. E. & Peterson, B. A. 1965, *ApJ*, 142, 1633
 Haardt, F. & Madau, P. 2012, *ApJ*, 746, 125
 Hauser, M. G. & Dwek, E. 2001, *ARA&A*, 39, 249
 Hauser, M. G. et al. 1998, *ApJ*, 508, 25
 Heitler, W. 1954, *Quantum theory of radiation* (Clarendon)
 Helgason, K. & Kashlinsky, A. 2012, *ApJ*, 758, L13
 Hopkins, A. M. 2004, *ApJ*, 615, 209
 Hopkins, A. M. & Beacom, J. F. 2006, *ApJ*, 651, 142
 Horiuchi, S., Beacom, J. F., & Dwek, E. 2009, *Phys. Rev. D*, 79, 083013
 Horiuchi, S., Beacom, J. F., Kochanek, C. S., Prieto, J. L., Stanek, K. Z., & Thompson, T. A. 2011, *ApJ*, 738, 154
 Hosokawa, T., Omukai, K., Yoshida, N., & Yorke, H. W. 2011, *Science*, 334, 1250
 Inoue, S., Salvaterra, R., Choudhury, T. R., Ferrara, A., Ciardi, B., & Schneider, R. 2010a, *MNRAS*, 404, 1938
 Inoue, S. et al. 2013, *arXiv:1301.3014*
 Inoue, Y. 2011a, *ApJ*, 733, 66
 —. 2011b, *ApJ*, 728, 11
 Inoue, Y., Inoue, S., Kobayashi, M. A. R., Totani, T., Kataoka, J., & Sato, R. 2011, *MNRAS*, 411, 464
 Inoue, Y. & Ioka, K. 2012, *Phys. Rev. D*, 86, 023003
 Inoue, Y., Totani, T., & Mori, M. 2010b, *PASJ*, 62, 1005
 Inoue for the CTA Consortium, Y. 2011, in *AGN Physics in the CTA Era (AGN 2011)*
 Iwata, I. et al. 2009, *ApJ*, 692, 1287
 Jelley, J. V. 1966, *Physical Review Letters*, 16, 479
 Kakuwa, J., Murase, K., Toma, K., Inoue, S., Yamazaki, R., & Ioka, K. 2012, *MNRAS*, 425, 514
 Karim, A. et al. 2011, *ApJ*, 730, 61
 Kauffmann, G., White, S. D. M., & Guiderdoni, B. 1993, *MNRAS*, 264, 201
 Kawai, N. et al. 2006, *Nature*, 440, 184
 Keenan, R. C., Barger, A. J., Cowie, L. L., & Wang, W.-H. 2010, *ApJ*, 723, 40
 Kistler, M. D., Yüksel, H., Beacom, J. F., Hopkins, A. M., & Wytthe, J. S. B. 2009, *ApJ*, 705, L104
 Kneiske, T. M., Bretz, T., Mannheim, K., & Hartmann, D. H. 2004, *A&A*, 413, 807
 Kneiske, T. M. & Dole, H. 2010, *A&A*, 515, A19
 Kobayashi, M. A. R., Inoue, Y., & Inoue, A. K. 2013, *ApJ*, 763, 3
 Kobayashi, M. A. R., Totani, T., & Nagashima, M. 2007, *ApJ*, 670, 919
 —. 2010, *ApJ*, 708, 1119
 Komatsu, E. et al. 2011, *ApJS*, 192, 18
 Kuhlen, M. & Faucher-Giguère, C.-A. 2012, *MNRAS*, 423, 862
 Labbé, I. et al. 2010, *ApJ*, 716, L103
 Lagache, G., Haffner, L. M., Reynolds, R. J., & Tufte, S. L. 2000, *A&A*, 354, 247
 Lefa, E., Aharonian, F. A., & Rieger, F. M. 2011a, *ApJ*, 743, L19
 Lefa, E., Rieger, F. M., & Aharonian, F. 2011b, *ApJ*, 740, 64
 Levenson, L. R. & Wright, E. L. 2008, *ApJ*, 683, 585
 Levenson, L. R., Wright, E. L., & Johnson, B. D. 2007, *ApJ*, 666, 34
 Mackey, J., Bromm, V., & Hernquist, L. 2003, *ApJ*, 586, 1
 Madau, P., Haardt, F., & Rees, M. J. 1999, *ApJ*, 514, 648
 Madau, P. & Pozzetti, L. 2000, *MNRAS*, 312, L9
 Makiya, R. et al. in preparation
 Malkan, M. A. & Stecker, F. W. 1998, *ApJ*, 496, 13
 Mannucci, F., Buttery, H., Maiolino, R., Marconi, A., & Pozzetti, L. 2007, *A&A*, 461, 423
 Massarotti, M., Iovino, A., & Buzzoni, A. 2001, *ApJ*, 559, L105

- Matsumoto, T. et al. 2005, *ApJ*, 626, 31
Matsuoka, Y., Ienaka, N., Kawara, K., & Oyabu, S. 2011, *ApJ*, 736, 119
Matsuura, S. et al. 2011, *ApJ*, 737, 2
Mazin, D. & Raue, M. 2007, *A&A*, 471, 439
McKee, C. F. & Tan, J. C. 2008, *ApJ*, 681, 771
McQuinn, M., Hernquist, L., Zaldarriaga, M., & Dutta, S. 2007, *MNRAS*, 381, 75
McWilliam, A. 1997, *ARA&A*, 35, 503
Mesinger, A. & Haiman, Z. 2007, *ApJ*, 660, 923
Meyer, M., Raue, M., Mazin, D., & Horns, D. 2012, *A&A*, 542, A59
Mirabel, I. F., Dijkstra, M., Laurent, P., Loeb, A., & Pritchard, J. R. 2011, *A&A*, 528, A149
Mortlock, D. J. et al. 2011, *Nature*, 474, 616
Murase, K., Dermer, C. D., Takami, H., & Migliori, G. 2012, *ApJ*, 749, 63
Nagashima, M., Gouda, N., & Sugiura, N. 1999, *MNRAS*, 305, 449
Nagashima, M., Yahagi, H., Enoki, M., Yoshii, Y., & Gouda, N. 2005, *ApJ*, 634, 26
Nagashima, M. & Yoshii, Y. 2004, *ApJ*, 610, 23
Oesch, P. A. et al. 2009, *ApJ*, 690, 1350
Oh, S. P. 2001, *ApJ*, 553, 25
Ono, Y., Ouchi, M., Shimasaku, K., Dunlop, J., Farrah, D., McLure, R., & Okamura, S. 2010, *ApJ*, 724, 1524
Ouchi, M. et al. 2004, *ApJ*, 611, 685
—, 2009, *ApJ*, 706, 1136
—, 2010, *ApJ*, 723, 869
Papovich, C. et al. 2004, *ApJS*, 154, 70
Pascale, E. et al. 2009, *ApJ*, 707, 1740
Pawlik, A. H., Schaye, J., & van Scherpenzeel, E. 2009, *MNRAS*, 394, 1812
Peacock, J. A. 1999, *Cosmological Physics* (Cambridge University Press)
Primack, J. R., Bullock, J. S., & Somerville, R. S. 2005, in *American Institute of Physics Conference Series*, Vol. 745, *High Energy Gamma-Ray Astronomy*, ed. F. A. Aharonian, H. J. Völk, & D. Horns, 23–33
Prochaska, J. X., Naumov, S. O., Carney, B. W., McWilliam, A., & Wolfe, A. M. 2000, *AJ*, 120, 2513
Raue, M. & Meyer, M. 2012, *MNRAS*, 426, 1097
Reddy, N. A., Steidel, C. C., Pettini, M., Adelberger, K. L., Shapley, A. E., Erb, D. K., & Dickinson, M. 2008, *ApJS*, 175, 48
Ricotti, M. & Ostriker, J. P. 2004, *MNRAS*, 352, 547
Robertson, B. E. 2010, *ApJ*, 713, 1266
Robertson, B. E., Ellis, R. S., Dunlop, J. S., McLure, R. J., & Stark, D. P. 2010, *Nature*, 468, 49
Rodighiero, G. et al. 2010, *A&A*, 515, A8
Salpeter, E. E. 1955, *ApJ*, 121, 161
Salvaterra, R. et al. 2009, *Nature*, 461, 1258
Schaerer, D. 2003, *A&A*, 397, 527
Schiminovich, D. et al. 2005, *ApJ*, 619, L47
Schneider, R., Omukai, K., Inoue, A. K., & Ferrara, A. 2006, *MNRAS*, 369, 1437
Shapley, A. E., Steidel, C. C., Pettini, M., Adelberger, K. L., & Erb, D. K. 2006, *ApJ*, 651, 688
Sol, H. et al. in press, *Astropart. Phys.*
Somerville, R. S., Gilmore, R. C., Primack, J. R., & Domínguez, A. 2012, *MNRAS*, 423, 1992
Somerville, R. S. & Primack, J. R. 1999, *MNRAS*, 310, 1087
Stark, D. P., Bunker, A. J., Ellis, R. S., Eyles, L. P., & Lacy, M. 2007, *ApJ*, 659, 84
Stecker, F. W., de Jager, O. C., & Salamon, M. H. 1992, *ApJ*, 390, L49
Stecker, F. W., Malkan, M. A., & Scully, S. T. 2006, *ApJ*, 648, 774
—, 2012, *ApJ*, 761, 128
Tanvir, N. R. et al. 2009, *Nature*, 461, 1254
Toma, K., Sakamoto, T., & Mészáros, P. 2011, *ApJ*, 731, 127
Totani, T., Kawai, N., Kosugi, G., Aoki, K., Yamada, T., Iye, M., Ohta, K., & Hattori, T. 2006, *PASJ*, 58, 485
Totani, T. & Takeuchi, T. T. 2002, *ApJ*, 570, 470
Totani, T., Yoshii, Y., Iwamuro, F., Maihara, T., & Motohara, K. 2001, *ApJ*, 550, L137
Vaccari, M. et al. 2010, *A&A*, 518, L20
Verma, A., Lehnert, M. D., Förster Schreiber, N. M., Bremer, M. N., & Douglas, L. 2007, *MNRAS*, 377, 1024
Wheeler, J. C., Sneden, C., & Truran, Jr., J. W. 1989, *ARA&A*, 27, 279
Wright, E. L. 2004, *New A Rev.*, 48, 465
Wright, E. L. & Reese, E. D. 2000, *ApJ*, 545, 43
Wyder, T. K. et al. 2005, *ApJ*, 619, L15
Xu, C. K. et al. 2005, *ApJ*, 619, L11
Yajima, H., Choi, J.-H., & Nagamine, K. 2011, *MNRAS*, 412, 411
Yajima, H., Umemura, M., Mori, M., & Nakamoto, T. 2009, *MNRAS*, 398, 715
Yoshida, M. et al. 2006, *ApJ*, 653, 988
Yoshida, N., Bromm, V., & Hernquist, L. 2004, *ApJ*, 605, 579
Yoshii, Y. & Peterson, B. A. 1994, *ApJ*, 436, 551
Younger, J. D. & Hopkins, P. F. 2011, *MNRAS*, 410, 2180
Yüksel, H., Kistler, M. D., Beacom, J. F., & Hopkins, A. M. 2008, *ApJ*, 683, L5

APPENDIX

COSMIC STAR FORMATION HISTORY

In this appendix, we briefly review the method of conversion to the CSFH from the measurement of the 1500 Å UV LD $\varrho_{\text{obs}}(z)$, for which there are two steps (see Kobayashi et al. 2013, for details). One is the correction for dust obscuration to derive the intrinsic LD $\varrho_{\text{int}}(z)$ and the other is the conversion of the intrinsic LD to the star formation rate density $\dot{\rho}_{\text{star}}(z)$. Dust obscuration correction and star formation rate conversion are given by

$$\varrho_{\text{int}}(z) = C_{\text{dust}}(z)\varrho_{\text{obs}}(z), \quad (\text{A1})$$

$$\dot{\rho}_{\text{star}}(z) = C_{\text{SFR}}(z)\varrho_{\text{int}}(z). \quad (\text{A2})$$

Hopkins (2004) assumed redshift-independent C_{dust} and C_{SFR} , while Bouwens et al. (2007) and Cucciati et al. (2012) assumed redshift-dependent C_{dust} but with redshift-independent C_{SFR} (see Bouwens et al. 2007; Cucciati et al. 2012, for details). However, these simple assumptions for all redshifts can cause an overestimation of the CSFH. Kobayashi et al. (2013) have recently proposed a new redshift dependent conversion method based on their semi-analytical galaxy formation model as

$$C_{\text{dust}}(z) = 2.983 \exp[-0.3056(1+z)] + 1, \quad (\text{A3})$$

$$C_{\text{SFR}}(z) = 10^{-28.01} [1 - 5.915 \times 10^{-5}(1+z) + 7.294 \times 10^{-4}(1+z)^2] M_{\odot} \text{ yr}^{-1} (\text{erg s}^{-1} \text{ Hz}^{-1})^{-1}. \quad (\text{A4})$$

Fig. 15 shows the CSFH converted from the observed 1500 Å LD using the methods developed by Hopkins (2004), Bouwens et al. (2007), Cucciati et al. (2012), and Kobayashi et al. (2013). The 1500 Å UV LD data used in Hopkins (2004) are from Giavalisco et al. (2004) and Massarotti et al. (2001). The expected CSFH from our baseline Mitaka model fits well to the CSFH following Kobayashi et al. (2013).

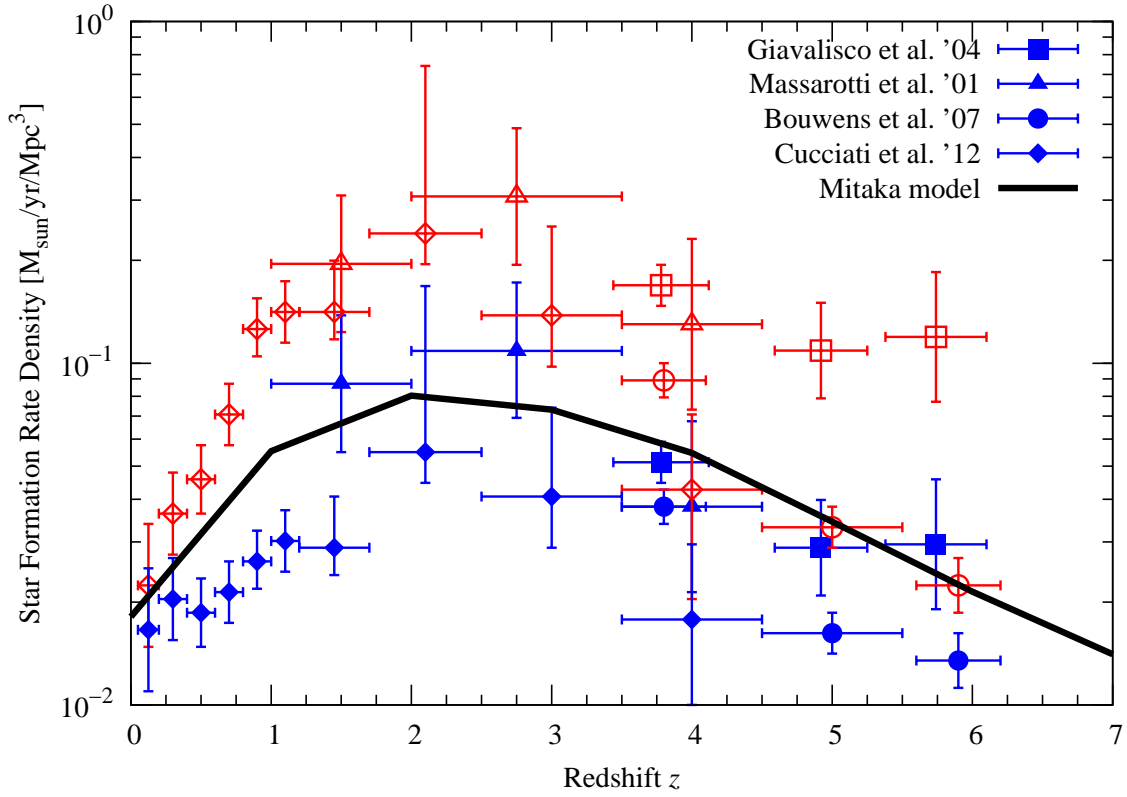


FIG. 15.— Cosmic star formation history. The solid curve shows the total in the baseline Mitaka model. Square, triangle, circle, and diamond symbols show the expected CSFH from the observed 1500 \AA LD by Giavalisco et al. (2004), Massarotti et al. (2001), Bouwens et al. (2007), and Cucciati et al. (2012) respectively. Open symbols are based on the conversion method by Hopkins (2004) for square and triangle symbols, by Bouwens et al. (2007) for circle symbols, and by Cucciati et al. (2012) for diamond symbols. Filled symbols are based on the method by Kobayashi et al. (2013). We converted the cosmology assumed in the original references to that assumed here.